

RESEARCH

Open Access



Platycodon grandiflorum-derived extracellular vesicles suppress triple-negative breast cancer growth by reversing the immunosuppressive tumor microenvironment and modulating the gut microbiota

Min Yang¹, Jia Guo¹, Jinxian Li¹, Shuyue Wang², Yuan Sun¹, Ying Liu¹ and Yinghua Peng^{1*}

Abstract

Despite the approval of several artificial nanotherapeutics for the treatment of triple-negative breast cancer (TNBC), significant challenges, including unsatisfactory therapeutic outcomes, severe side effects, and the high cost of large-scale production, still restrict their long-term application. In contrast, plant-derived extracellular vesicles (PEVs) exhibit promising potential in cancer therapy due to their negligible systemic toxicity, high bioavailability and cost-effectiveness. In this study, we developed an alternative strategy to inhibit TNBC via *Platycodon grandiflorum* (PG)-derived extracellular vesicles (PGEVs). The PGEVs were isolated by ultracentrifugation and sucrose gradient centrifugation method and contained adequate functional components such as proteins, lipids, RNAs and active molecules. PGEVs exhibited remarkable stability, tolerating acidic digestion and undergoing minimal changes in simulated gastrointestinal fluid. They were efficiently taken up by tumor cells and induced increased production of reactive oxygen species (ROS), leading to tumor cell proliferation inhibition and apoptosis, particularly in the TNBC cell line 4T1. Additionally, PGEVs facilitated the polarization of tumor-associated macrophages (TAMs) toward M1 phenotype and increased the secretion of pro-inflammatory cytokines. Further in vivo investigations revealed that PGEVs efficiently accumulated in 4T1 tumors and exerted significant therapeutic effects through boosting systemic anti-tumor immune responses and modulating the gut microbiota whether administered orally or intravenously (i.v.). In conclusion, these findings highlight PGEVs as a promising natural, biocompatible and efficient nanotherapeutic candidate for treating TNBC.

Keywords *Platycodon grandiflorum*, Plant-derived extracellular vesicles, TNBC, Tumor immunotherapy, Gut microbiota modulation

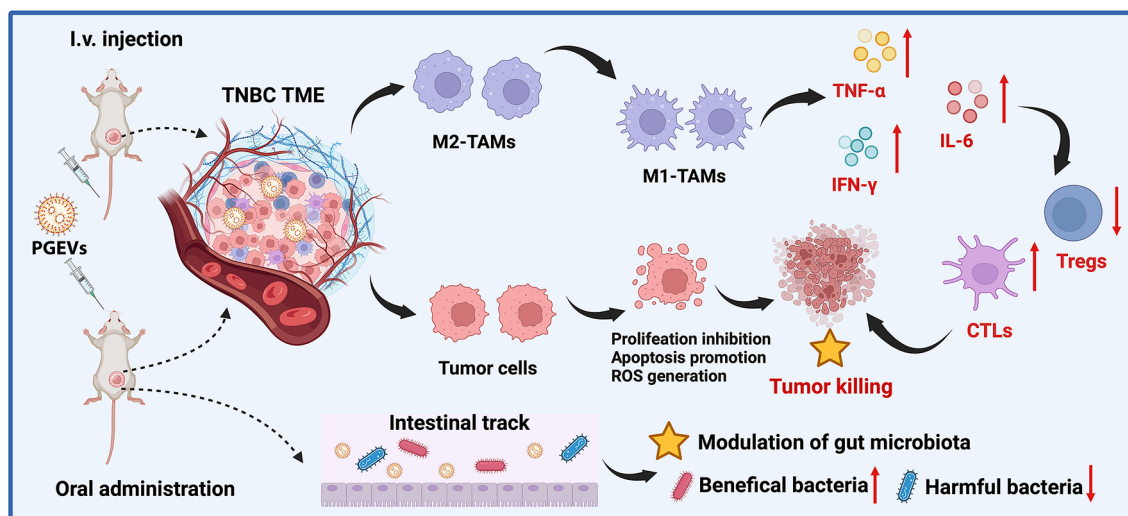
*Correspondence:

Yinghua Peng
pengyinghua@caas.cn

Full list of author information is available at the end of the article



© The Author(s) 2025. **Open Access** This article is licensed under a Creative Commons Attribution-NonCommercial-NoDerivatives 4.0 International License, which permits any non-commercial use, sharing, distribution and reproduction in any medium or format, as long as you give appropriate credit to the original author(s) and the source, provide a link to the Creative Commons licence, and indicate if you modified the licensed material. You do not have permission under this licence to share adapted material derived from this article or parts of it. The images or other third party material in this article are included in the article's Creative Commons licence, unless indicated otherwise in a credit line to the material. If material is not included in the article's Creative Commons licence and your intended use is not permitted by statutory regulation or exceeds the permitted use, you will need to obtain permission directly from the copyright holder. To view a copy of this licence, visit <http://creativecommons.org/licenses/by-nc-nd/4.0/>.

Graphical Abstract**Introduction**

Triple-negative breast cancer (TNBC), known for its high invasiveness, metastasis, recurrence, and mortality rates, represents a serious threat to young women [1]. Although chemotherapy remains the major available approach for TNBC treatment, its effectiveness is limited in a significant portion of patients because of its non-specific drug distribution and severe adverse effects [2]. Studies have indicated that TNBC exhibits a higher tumor mutation burden (TMB), increasing the likelihood of benefiting from tumor immunotherapy. A higher TMB can increase neoantigen production, thereby increasing the probability of tumor cells being recognized and attacked by the immune system [3]. However, challenges such as low tumor immunogenicity and the presence of the immunosuppressive tumor microenvironment (TME) persistently impede the effectiveness of immunotherapeutic strategies for TNBC [4]. Therefore, novel approaches that bolster tumor immunogenicity and reverse the immunosuppressive TME are essential for enhancing the immunotherapy outcomes of TNBC.

Driven by the advancements in biomaterials and nanobiotechnology, nanotherapeutics have gained considerable attention in the field of TNBC immunotherapy, which aims to improve precision and effectiveness by leveraging the distinctive properties of synthetic nanomaterials [5]. However, despite these advancements, only a limited number of nanotherapeutics are approved for clinical application. This is largely attributed to challenges such as low long-term treatment efficiency, concerns regarding biocompatibility and issues related to residues of toxic catalysts and organic solvents [6, 7]. In recent years, scientists have advocated prioritizing patient-centric approaches (disease first) over traditional

methods that emphasize material synthesis (formula first) [8]. Consequently, natural products, especially those sourced from edible plants, including vegetables, fruits and medicinal plants, have become increasingly attractive as therapeutic options for tumor treatment [9]. Plant-derived extracellular vesicles (PEVs) are nanovesicles with lipid bilayer membrane structures, and contain proteins, lipids, nucleic acids and active molecules [10]. Unlike synthetic nanomaterials, PEVs are natural bioactive substances from plants, which have gained increasing attention and demonstrated excellent efficacy in treating various diseases, including cancers [11].

For a long time, research on extracellular vesicles (EVs) has focused primarily on those of mammalian origin, which have been extensively utilized in biochemical and pharmacological research [12]. Despite their promising potential in biological applications, the clinical translation of mammalian EVs faces significant challenges, such as low yield, limited resources, difficulties in large-scale production and time-consuming isolation processes [13]. Moreover, it is noteworthy that the use of mammals as a source of vesicles may trigger host immune responses, potentially causing biohazards [14]. Nevertheless, the discovery of PEVs and the elucidation of their functional mechanisms provide a promising alternative to address these issues. Unlike EVs derived from mammalian sources, PEVs isolated from plants present numerous advantages, including significant mass production, enhanced biocompatibility and low cost [15]. These natural PEVs contain abundant bioactive ingredients from source plants, which have demonstrated beneficial effects on immune regulation and anti-tumor activity [16]. For example, ginseng-derived PEVs induced M1 macrophage polarization through toll-like receptor 4 (TLR4) and

myeloid differentiation antigen 88-mediated signaling, thereby restricting tumor growth [17]. PEVs extracted from tea flowers inhibited breast cancer growth by modulating the gut microbiota following both oral and intravenous (i.v.) administration [18]. Oral administration of these PEVs was found to be relatively safer than i.v. injection, as it tended to preserve blood cell counts and mitigate hepatorenal toxicity. Despite many advantages, the clinical use of PEVs still faces challenges because the understanding of PEVs remains in their early stage. Comprehensive investigations into the physical and chemical properties, composition, biosafety, biodistribution and other essential characteristics of PEVs are essential for accelerating their clinical application.

Platycodon grandiflorum (PG) is a perennial herb belonging to the *Grandiflorum* family. With advancements in modern pharmacology, research on PG has expanded significantly, exploring its diverse therapeutic properties, including anti-inflammatory, antioxidant, liver-protective, anti-tumor and immune-modulatory effects [19]. Among them, its anti-tumor and immunomodulatory effects are particularly prominent [20]. Platycodin D (PD), the primary active component of PG, has been reported to inhibit the growth of various tumors, including glioma, oral cancer, breast cancer, gastric cancer, non-small cell lung cancer, liver cancer, leukemia melanoma and bladder cancer [21, 22]. From a mechanistic perspective, the anti-cancer mechanisms of PG are diverse and primarily involve the inhibition of tumor cell proliferation, migration and invasion, the induction of tumor cell apoptosis, and antiangiogenic effects [23, 24]. Notably, the anti-tumor effects of PG can be achieved via immunomodulation. For instance, PD polysaccharides activate macrophages by binding to TLR4 on their surface and thereby regulating the function of macrophages through the TLR4/NF- κ B signaling pathway [25]. PD combined with other traditional Chinese medicines modulates tumor-associated macrophages (TAMs), reduces the secretion of TGF- β and IL-10, and enhances the cytotoxicity of natural killer (NK) cells to tumor cells, resulting in the inhibition of gastric cancer [26]. Moreover, PG enhances the T cell-mediated immune response by downregulating the expression of PD-1 on cytotoxic T lymphocytes (CTLs) and has potent immunotherapeutic efficacy against tumors [27]. However, the unsatisfied solubility and bioavailability (only 1.89%) of PD result in limited therapeutic effect [28], which hinder its clinical application. More importantly, the efficacy of a single compound is inferior to that of a whole plant extract because there may be positive interactions between the different components [29]. Unlike single component, PEVs contain a range of bioactive substances (proteins, lipids, nucleic acids and active molecules), enabling broader therapeutic effects based on multiple targets

and pathways. Furthermore, owing to their distinctive composition and structure, PEVs are capable of encapsulating and safeguarding their bioactive cargo, while also facilitating the release and internalization of these contents within target cells, which can overcome the challenges associated with low solubility and bioavailability that are commonly encountered with compounds such as saponins. To our knowledge, there are no reports on the immunomodulatory and anti-tumor functions of PG-derived extracellular vesicles (PGEVs). It also remains unclear whether PGEVs possess the ability to inhibit TNBC and the underlying mechanisms.

In the current work, we extracted PGEVs from PG through ultracentrifugation and sucrose gradient centrifugation method, characterized their stability in simulated gastrointestinal fluid and determined their protein, lipid, RNA and molecule components (Scheme 1A). The efficiency of the internalization of PGEVs by different cells in vitro and their biodistribution characteristics via both oral and i.v. routes in vivo were investigated. Furthermore, their anti-tumor activity and the ability to induce TAM polarization were evaluated in vitro. Finally, we conducted a comparative assessment of the therapeutic efficacy of PGEVs and their impact on immune activation and gut microbiota modulation in TNBC mice model after both oral and i.v. administration (Scheme 1B).

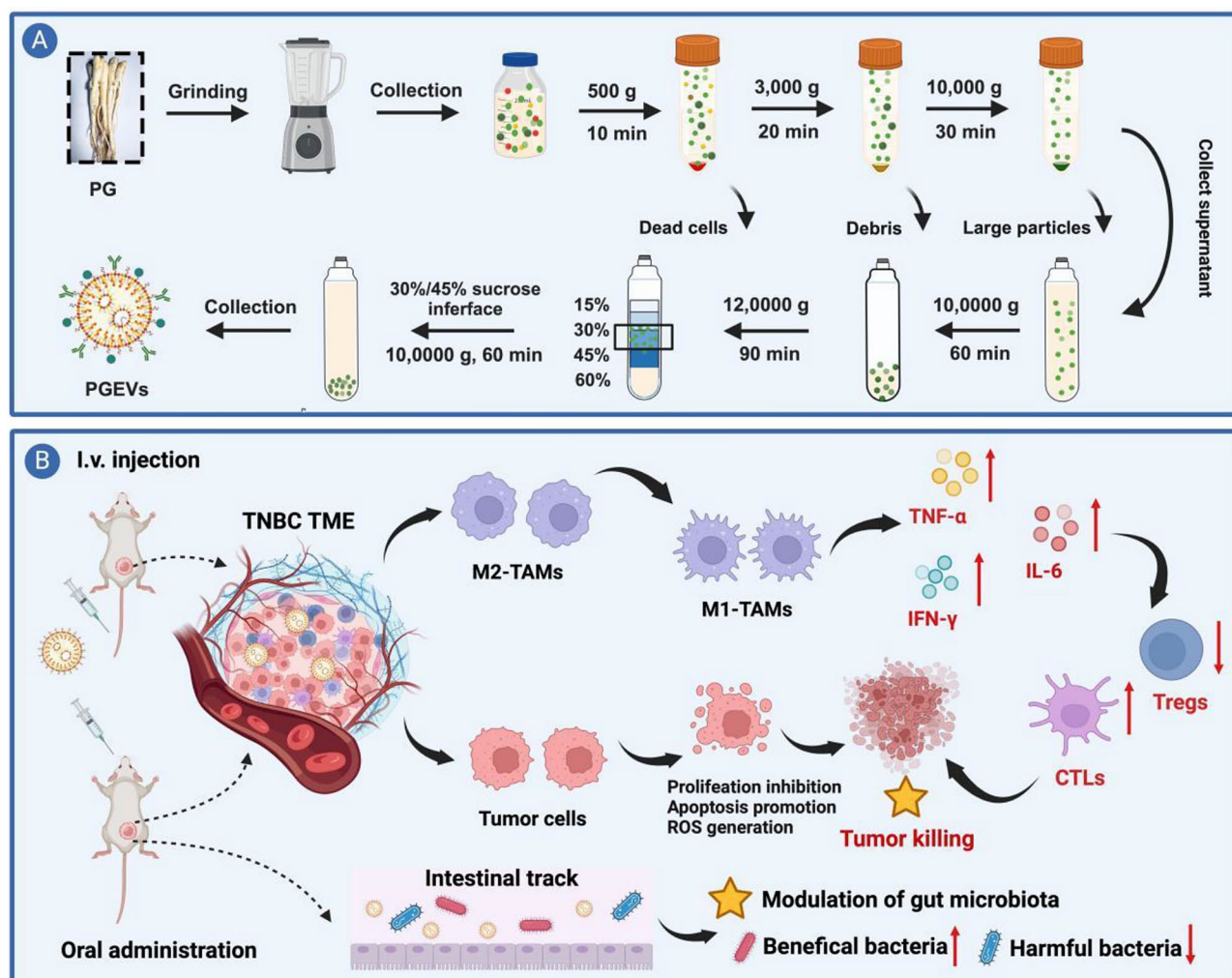
Materials and methods

Isolation and purification of PGEVs

Fresh PG was obtained from a local farm (Jilin, China). After being washed with deionized water, the PG was ground with a juicer (Hurom, South Korea) to obtain PG juice. The juice was subsequently centrifuged at $500 \times g$ for 10 min, $3000 \times g$ for 20 min and $10,000 \times g$ for 30 min at 4°C to eliminate dead cells, debris and large particles, respectively. The obtained supernatant was subsequently ultracentrifuged at $100,000 \times g$ for 1 h (Beckman Coulter, USA), after which the pellets were resuspended in PBS. The pellets were subsequently transferred to density gradient sucrose solutions (15%, 30%, 45% and 60%, w/v) and ultracentrifuged at $120,000 \times g$ for 1.5 h at 4°C . Finally, the PGEVs were collected from the 30/45% sucrose interface, and the excess sucrose was removed by ultracentrifugation at $100,000 \times g$ for 1 h. A BCA assay kit (Thermo Fisher, Waltham, MA, USA) was used to determine the protein concentration of PGEVs. Finally, the obtained PGEVs were stored at -80°C .

Characterization of PGEVs

For morphology measurements, PGEVs were dropped onto carbon-coated copper grids and stained with 2% uranyl acetate for 30 s. Then, the dried samples were imaged via a transmission electron microscopy (TEM) (JEOL, Tokyo, Japan). The PGEVs were diluted to the



Scheme 1 The extraction process of PGEVs and their mechanisms in treating TNBC via oral administration and i.v. injection. **(A)** Extraction process of PGEVs through ultracentrifugation and sucrose gradient centrifugation method. **(B)** Anti-tumor mechanisms of PGEVs against TNBC via oral and i.v. administration in vivo

proper concentration, and their particle size and concentration were measured via nanoflow cytometry (NanoFCM, Xiamen, China) and the nanocoulter counter [30] (Resun Technology, Shenzhen, China). The zeta potential of the PGEVs was detected by the nanocoulter counter. In addition, the compositions of PGEVs were identified. In detail, 10 μL of PGEVs was mixed with 5 \times loading buffer and incubated for 15 min at 100 $^{\circ}\text{C}$. The protein samples were then separated on 15% SDS-PAGE gel (Epizyme, Shanghai, China) and stained with Coomassie brilliant blue dye (Beyotime, Shanghai, China). The stained gel was then visualized using a multifunctional gel imaging system (Tanon, Shanghai, China). Total RNA was extracted from PGEVs via a nucleic acid extraction kit (Tiangen, Beijing, China). After electrophoresis on a 1.5% agarose gel, the gel was stained with SYBR Green and the RNA bands were observed under ultraviolet light. The high performance liquid

chromatography (HPLC) was conducted to detect the PD content in PGEVs. By comparing the retention time and peak area with the standard product, the PD content in PGEVs was accurately calculated.

Proteomic analysis of PGEVs

For proteomic analysis, 20 μL of PGEVs was incubated with lysis buffer for protein extraction. The protein mixture was digested with trypsin and desalted on a Strata X SPE column. These peptides were then separated via an EASY-nLC 1200 UPLC system (Thermo Fisher, USA). An Orbitrap Exploris 480 was used to analyze the separated peptides. The MS/MS data were processed via the DIA-NN search engine (v1.8).

Lipidomic analysis of ADNVs

The PGEVs samples were mixed with total lipid extraction solvent and phase separated with ultrapure water.

The organic layer in the upper layer was collected and evaporated, and the residue from phase B was analyzed using an LC-ESI-MS/MS system (UPLC, ExionLC AD; MS, ATRAP 6500 + System).

Stability evaluation of PGEVs in vitro

Changes in the particle size and concentration of PGEVs after incubation with different biological lipids were measured using a nanoflow cytometry. In detail, 5 μ L of PGEVs was mixed with 45 μ L of PBS, 10% FBS, stimulated intestinal fluid (SIF) or stimulated gastric fluid (SGF) and incubated at 37 °C for 1 h, 3 h, 6 h, 12 h, 24 h or 48 h. Then, this mixture was diluted to an appropriate concentration, and the nanoflow cytometry was used to detect their changes in mean size and size distribution.

Cellular uptake of PGEVs

Fluorescence imaging and flow cytometry were conducted to detect the uptake of PGEVs by macrophages and tumor cells. The fluorescent dye DiI (Beyotime) was used to label PGEVs (DiI-PGEVs). 4T1 cells, A549 cells and Raw 264.7 cells were respectively cultured in 6-well plates overnight and treated with DiI-PGEVs for different durations. For observation under fluorescence microscopy, the cells were fixed with 4% paraformaldehyde, and the nuclei were stained with DAPI. The cells were subsequently imaged with a fluorescence microscope. For quantitative analysis through flow cytometry (BD, USA), the cells were collected and counted, after which at least 10,000 stained cells were tested to obtain the percentage of DiI⁺ cells.

Anti-tumor activity of PGEVs in vitro

The inhibitory effect of PGEVs on tumor cells was investigated by CCK-8 assay in vitro. PGEVs at protein concentrations ranging from 12.5 μ g/mL to 100 μ g/mL were added to 4T1 cells and A549 cells in 96-well plates and co-incubated at 37 °C for 24 h and 48 h. Then, 10 μ L of CCK-8 working solution (KeyGEN Biotechnology, Nanjing, China) in 100 μ L of fresh medium was added, and the mixture was cultured for another 1–2 h. Finally, the OD values at 450 nm were detected with a microplate reader (Biotech, USA) to determine the cell viabilities.

Pro-apoptosis property of PGEVs in vitro

The in vitro pro-apoptotic property of PGEVs on different cells was detected using Annexin V-FITC/PI kit. 50 μ g/mL or 100 μ g/mL of PGEVs were added to 4T1, A549 or Raw 264.7 cells in 6-well plate and cultured for 48 h. After washing with PBS, 10 μ L of Annexin V-FITC and 5 μ L of PI were added to the collected cells and incubated for 15 min in the dark. These cells were then detected immediately using flow cytometry.

Plate colony formation assay

600 4T1 cells or A549 cells were seeded in 6-well plates. The medium was discarded after cultured for 24 h, and then 50 μ g/mL or 100 μ g/mL PGEVs in fresh medium were added to the cells. Two weeks later, the cells were stained with 0.1% crystal violet. The colony formation ability was evaluated by comparing the colony density.

Impact of PGEVs on ROS generation

Intracellular ROS production was detected with the fluorescence probe DCFH-DA (Beyotime). In detail, 4T1 or A549 cells in 12-well plates were treated with 50 μ g/mL or 100 μ g/mL PGEVs. For fluorescence observation, after 24 h of incubation, DCFH-DA probe in FBS-free medium was added to each well, and incubated at 37 °C for 20 min. Then, the nuclei were stained with Hoechst 33258, the cells were imaged with a fluorescence microscope. For ROS quantitative analysis, the cells at the same counts were collected and stained with DCFH-DA probe, the fluorescence intensity of DCF was detected with a microplate reader (excitation wavelength :488 nm, emission wavelength: 525 nm). The relative fluorescence intensity of DCF were normalized to control group.

The polarization of TAMs in vitro

A 6-well transwell coculture system with a 0.4 μ m pore size (Labsselect, Hefei, China) was used to imitate TAMs. Briefly, PGEVs (25 μ g/mL or 50 μ g/mL) -treated Raw 264.7 cells were seeded in the upper chamber and co-cultured with 4T1 cells or A549 cells in the lower chamber for 24 h. Total RNA was extracted from the treated Raw 264.7 cells via a nucleic acid extraction kit (Tiangen), after which a reverse transcription kit (Abm, Canada) was used to reverse-transcribe the RNA into cDNA. qRT-PCR experiments were conducted to assess the mRNA expression levels of M1 markers (iNOS, TNF- α , IL-6 and IL-12) and M2 marker (CD206), the mRNA expressions were normalized to those of GAPDH.

The supernatant in the upper chamber was collected, and the dead cells and large vesicles were removed through centrifugation. The cytokines TNF- α , IL-6, IL-4 and IL-10 released from the co-cultured Raw 264.7 cells were subsequently detected using enzyme-linked immunosorbent assay (ELISA, ABclonal, Wuhan, China) according to the manufacturer's protocol.

The expression level of the M1 marker protein CD86 was measured using flow cytometry. Raw 264.7 cells were collected and incubated with fluorescence labeled-CD86 antibody at room temperature for 30 min in the dark. The percentage of CD86⁺ cells was then measured by flow cytometry.

Immunofluorescence staining experiments were also conducted to evaluate the expression levels of the M1 marker proteins CD86 and iNOS. Raw 264.7 cells were

fixed and blocked. Then, the cells were incubated with primary antibodies against CD86 and iNOS at 4 °C overnight and with the corresponding secondary antibodies for 1 h at room temperature. After the nuclei were stained with DAPI for 6 min, a fluorescence microscope was employed to detect the expressions of these proteins.

Biodistribution of PGEVs in vivo

To evaluate the biodistribution of PGEVs in vivo, PGEVs were incubated with the fluorescent dye DiD at 37 °C for 1 h, after which DiD-labeled PGEVs (DiD-PGEVs) were isolated by ultracentrifugation and resuspended in PBS. Four-week-old Balb/C nude mice were orally administered or i.v. injected with DiD-PGEVs (5 mg/kg per mouse). Mice given PBS served as control group. At different time points (1 h, 3 h, 6 h, 12 h, 24 h and 48 h), DiD fluorescence was tracked and recorded with an animal in vivo imaging system (Tanon ABL X5, Shanghai, China). The mice were executed at different time points, and the major organs (heart, liver, spleen, lung, and kidney), brains and intestines were imaged by the same imaging system mentioned above. The quantitative results were conducted using the image analysis software provided by the in vivo imaging system.

Biosafety evaluation of PGEVs in vivo

ICR mice at 6-week-old were randomly divided into three groups: control, PGEVs (oral, low), PGEVs (oral, high), PGEVs (i.v., low) and PGEVs (i.v., high). The low dose was 5 mg/kg PGEVs per mouse, and the high dose was 10 mg/kg PGEVs per mouse. These PGEVs were given every other day for 7 doses. Then, blood from the mice was collected, and the concentrations of alanine aminotransferase (ALT), aspartate aminotransferase (AST), urea nitrogen (BUN) and creatinine (CREA) in the serum were measured. The major organs (heart, liver, spleen, lung, and kidney) and the brain were subsequently collected for further H&E staining.

Tumor targeting and anti-tumor effect of PGEVs in vivo

For tumor targeting assessment, 100 µL of PBS containing 10^6 4T1 cells was subcutaneously implanted into the left back of the Balb/C mice to establish TNBC tumor-bearing mice model. When the tumor volume reached approximately 70 mm³, the mice were orally or i.v. injected with DiD-PGEVs (5 mg/kg per mouse), the mice were executed at different time points, and the main organs, brains and tumors were harvested. Finally, the animal in vivo imaging system mentioned above was used to track the fluorescent signal.

For tumor treatment, the tumor-bearing mice were randomly divided into five groups: control, PGEVs (oral, low), PGEVs (oral, high), PGEVs (i.v., low) and PGEVs (i.v., high). The low dose was 5 mg/kg PGEVs per mouse,

and the high dose was 10 mg/kg PGEVs per mouse. PGEVs were given every two days for 7 doses. The following formula was used to measure the tumor volumes: $V = 1/2 * (\text{longest dimension} * \text{shortest dimension}^2)$. The mice from different groups were executed and the tumor tissues were collected and weighed at the end of treatment. The tumors were fixed and sectioned into 4 µm slices. The slices were subsequently stained with TUNEL (Beyotime) and antibodies against Ki67 and CD31 (Abcam) and imaged using a scanner.

Immune response analysis in vivo

For the assessment of immune responses in PGEVs treated mice, the mice were sacrificed, and serum and tumor tissues were collected. To analyze immune cell infiltration in tumors using flow cytometry, tumor tissues were enzymatically digested under continuous shaking at 37 °C. The obtained cell suspensions were filtered to achieve single-cell preparations. For labeling M1 macrophages, the cells were stained with antibodies against CD86 and F4/80. For labeling CD8⁺ cytotoxic T lymphocytes (also known for CTLs), the cells were stained with antibodies against CD3 and CD8. The percentage of CD86⁺F4/80⁺ cells and CD3⁺CD8⁺ cell were detected via flow cytometry.

Immunofluorescence staining was performed to observe the reprogramming effect of TAMs and T cell infiltration. The fixed tumor tissues were sliced and stained with CD86, CD206, CD3, CD8, Foxp3 and PD-1 antibodies. After the nuclei were stained with DAPI, the slices were imaged via a scanner.

The serum from the mice in different groups was collected and diluted to proper concentration. Then, the ELISA kit was used to detect the concentrations of cytokines (TNF-α, IL-6 and IFN-γ) according to the manufacturer's instructions.

Gut microbiota analysis

The feces from different PGEVs treated mice were collected, and the DNA was extracted using the CTAB following the manufacturer's recommendation. PCR experiment was used to amplify a specific region of the bacterial 16S ribosomal RNA gene. The samples were then sequenced on an Illumina NovaSeq platform according to the manufacturer's recommendation, provided by LC-Bio Technology Co., Ltd. (Hangzhou, China).

Statistical analysis

The data are presented as the mean ± standard deviation (SD). The statistical significance was performed by one-way analysis of variance (ANOVA) followed by the Tukey's post-hoc test for multiple comparisons.

Statistical significance was defined as follows: *** $P < 0.001$, ** $P < 0.01$, * $P < 0.05$; ### $P < 0.001$, ## $P < 0.01$, # $P < 0.05$.

Results

Identification and characterization of PGEVs

PGEVs were isolated from fresh PG by ultracentrifugation and sucrose gradient centrifugation method. Driven by the sucrose gradient, the PGEVs were deposited

primarily at the 30%/45% interface. TEM was employed to character the morphology of the PGEVs (Fig. 1A). The TEM images clearly revealed that the PGEVs were typical spherical nanovesicles. Two methods were used to detect the particle size of the PGEVs. The nanoflow cytometry results demonstrated that the mean diameter of the PGEVs was 73.0 nm and the median diameter was 64.8 nm (Fig. 1B). The nanocoulter counter measured

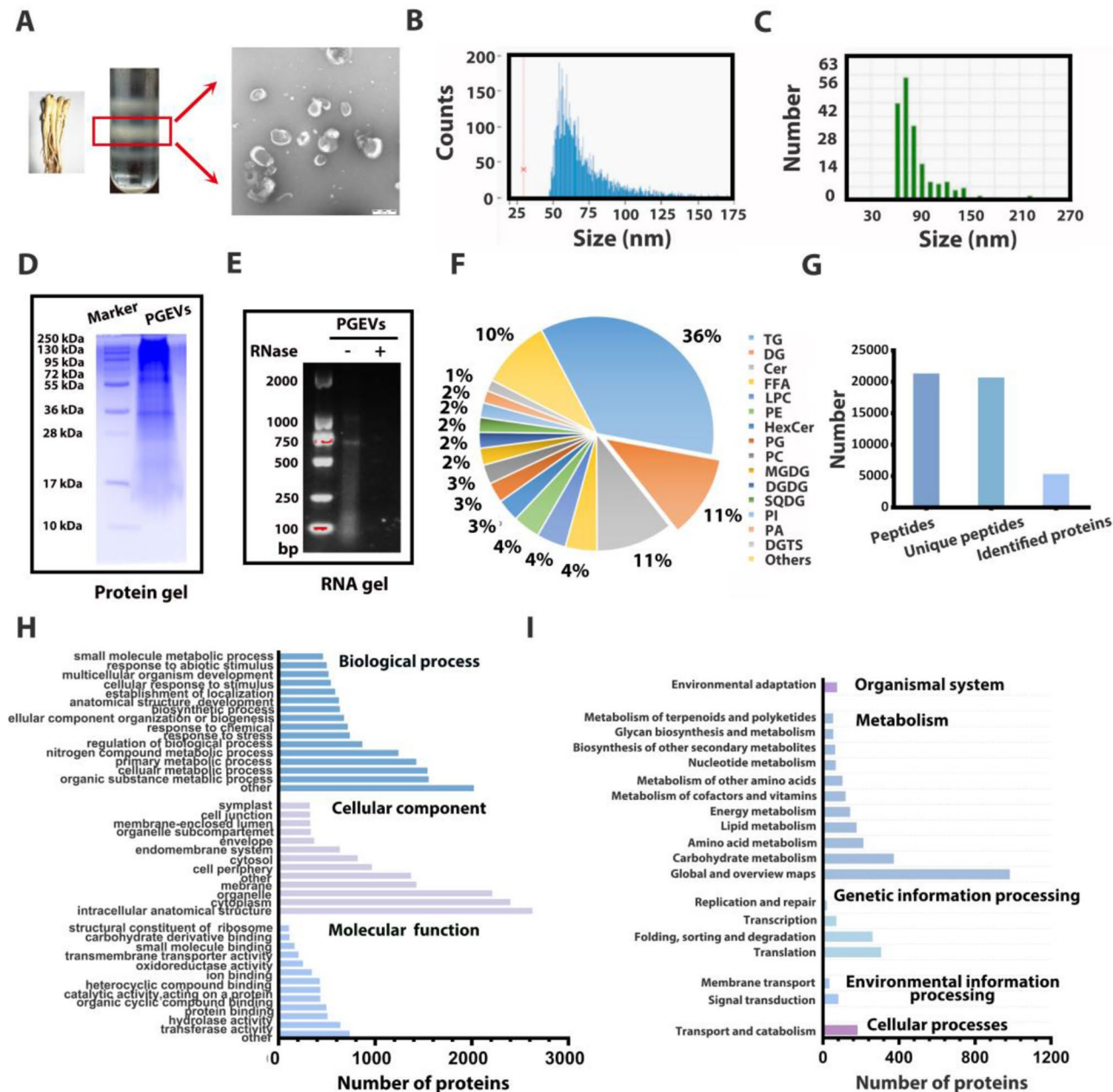


Fig. 1 Identification and characterization of PGEVs. **(A)** TEM images of PGEVs, scale bar: 200 nm. Size distribution of PGEVs detected by nanoflow cytometry **(B)** and nanocoulter counter **(C)**. **(D)** SDS-PAGE gel electrophoresis of PGEVs. The proteins in PGEVs were separated via 15% SDS-PAGE and stained with Coomassie blue dye. **(E)** Agarose gel electrophoresis of PGEVs. The RNA extracted from PGEVs was treated with or without RNase and run on a 1.5% agarose gel. Lipid compositions **(F)** and protein summary **(G)** of PGEVs. GO secondary classification statistical charts **(H)** and KEGG annotated statistical charts **(I)** of proteins in PGEVs

that the mean size and median size of the PGEVs were 74.0 nm and 74.0 nm, respectively (Fig. 1C). The zeta potential is a significant parameter for evaluating the stability of nanoparticles. According to the results from the nanocoulter counter, the zeta potential of PGEVs was -19.23 mV (Fig. S1), which was conducive to their medical application in vivo. PEVs usually contain proteins and RNAs. The SDS-PAGE gel electrophoresis was conducted to detect the protein distribution in PGEVs. The results revealed that the molecular weights of the major proteins ranged from 30 kDa to 130 kDa (Fig. 1D). The agarose gel electrophoresis results demonstrated that the nucleic acids within PGEVs were mainly small RNAs, as proven by the total degradation of these nucleic acids after treatment with RNase (Fig. 1E). In addition, the PD content in PGEVs (17.1 $\mu\text{g}/\text{mL}$) was detected through HPLC (Fig. S2).

Lipidomic analysis was conducted to identify the lipid composition of PGEVs. As shown in Fig. 1F and Table S1, the major lipid components in PGEVs were triglyceride (TG, 35.6%), diacylglycerol (DG, 11.4%) and ceramide (Cer, 10.6%). According to previous report, Cer is a crucial component known for its role in facilitating or inducing membrane curvature during the formation and secretion of EVs [31]. The presence of Cer in PGEVs proved the natural secretion of PGEVs from PG. A considerable proportion of phospholipids, including lysophosphatidylcholine (LPC, 4.1%), phosphatidylethanolamine (PE, 3.7%), phosphatidylglycerol (PG, 2.8%) and phosphatidylcholine (PC, 2.7%), were detected in PGEVs, which was consistent with the fact that PEVs are enriched in phospholipids. Phospholipids play a crucial role in promoting the neural cell differentiation and activating the neutrophils and macrophages. Additionally, they participate in regulating immune responses, including their recognition by TLRs and the activation of immune cells [32]. These results prompted us to speculate the potential participation of PGEVs in immunomodulatory processes. Furthermore, monogalactosyldiacylglycerol (MGDG) and digalactosyldiacylglycerol (DGDG) accounted for 2.3% and 2.2% of the total lipids in PGEVs, respectively, which were usually utilized to stabilize phospholipids during freeze-thawing and freeze-drying [33]. MGDG is particularly notable for its strong binding affinity to the asialoglycoprotein receptor (ASGPR) that highly expressed on the surface of tumor cells, which makes it beneficial for improving the targeted delivery of bioactive molecules to tumor sites [34]. Phosphatidic acid (PA), constituting 1.7% of the total lipids in PGEVs, participates in various biological functions and processes, including cell proliferation, transformation and differentiation. It also influences the uptake of PEVs by inducing cytoskeleton rearrangement [35]. Additionally, the above lipids found in PGEVs are amphiphilic, which are crucial for

maintaining the structural integrity and stability of these vesicles. The analysis of lipid composition contributes to elucidating the origin and function of PGEVs.

Proteomic analysis was conducted to analyze the compositions of proteins in PGEVs. The results revealed the presence of 5296 proteins in PGEVs (Fig. 1G), including aquaporin-like proteins, ribosomal proteins, transmembrane proteins, and the plasma membrane. The heat shock proteins 70 and 90 (HSP 70 and HSP 90), as well as glutathione transferase and glyceraldehyde-3-phosphate dehydrogenase (GAPDH), were detected in PGEVs, which have been frequently reported in previous studies on PEVs [36]. RNA-binding proteins such as argonaute (AGO) were also identified in PGEVs. AGO proteins, in association with small RNAs (sRNAs), are involved in gene silencing via complementary sequences, potentially influencing the packaging of small RNAs in PGEVs. This finding suggest that PGEVs, as functional vesicles, may participate in cargo transportation within the PG [37]. The biological functions of the above proteins were analyzed through GO database (Fig. 1H). They were classified into three categories: biological process, cellular component and molecular function. In addition, KEGG analysis displayed that the proteins in PGEVs were associated primarily with the organismal system, metabolism, genetic information processing, environmental information processing and cellular components (Fig. 1I). Overall, these results revealed that PGEVs contained abundant lipids and proteins.

Stability and cellular uptake of PGEVs in vitro

Among all routes of administration, oral administration is regarded as the most convenient method because of its minimal requirement for additional labor or equipment, low cost and high patient compliance. However, the harsh conditions in the gastrointestinal tract (GIT), characterized by strong stomach acidity and active digestive enzymes, presents significant challenges for the oral administration of biomaterials. PGEVs were incubated with PBS, 10% FBS, SIF or SGF for various durations to evaluate their stability in GIT. Changes in their particle size and size distribution were detected using nanoflow cytometry, as presented in Fig. 2A-D and Fig. S3. The particle size of PGEVs remained stable in PBS, 10% FBS and SGF at all time points. However, a slight decrease in particle size was observed in SIF after 48 h of incubation. These findings indicated that PGEVs were able to maintain their integrity and resist digestion while passing through the GIT for at least 24 h.

For effective tumor treatment, it is crucial that tumor cells efficiently internalize PGEVs, as the active components of natural nanoparticles exert their therapeutic effects mainly within the cells. To assess the cellular uptake of PGEVs, DiI-labeled PGEVs (DiI-PGEVs) were

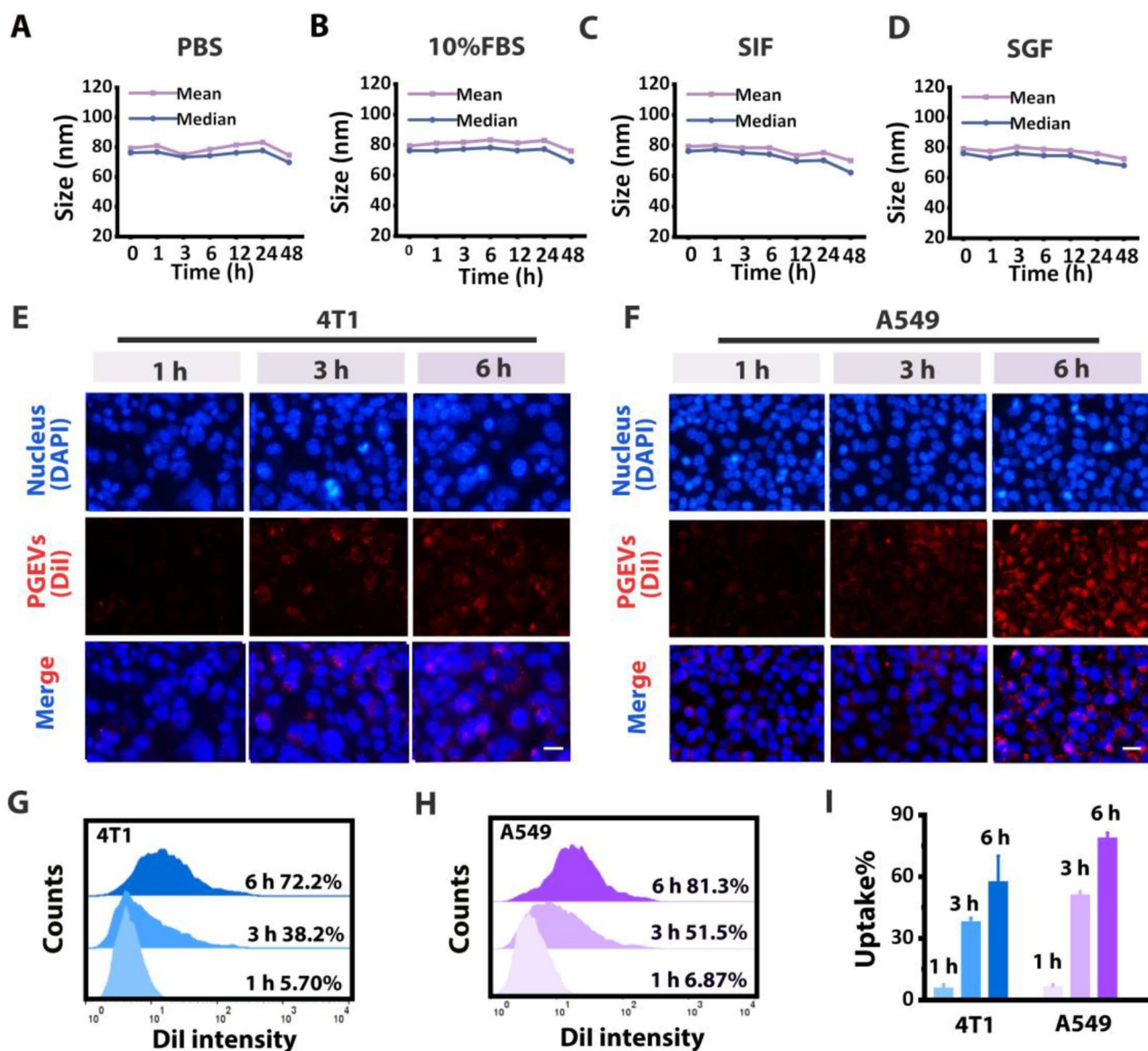


Fig. 2 Stability and cellular uptake of PGEVs in vitro. Changes in the mean particle sizes and median sizes of PGEVs after incubation in PBS (A), 10% FBS (B), SIF (C) or SGF (D) at 37 °C for 1 h, 3 h, 6 h, 12 h, 24 h, or 48 h. Representative fluorescence images of DiI-PGEVs treated 4T1 cells (E) and A549 cells (F) for 1 h, 3 h, or 6 h, scale bar: 50 μ m. The uptake efficiency of DiI-PGEVs in 4T1 cells (G) and A549 cells (H) was tested using flow cytometry and the corresponding quantitative analysis (I)

incubated with 4T1 and A549 cells, and their internalization was observed using fluorescence microscopy. As indicated in Fig. 2E and F, the internalization of PGEVs was observed to be time-dependent. After 6 h of incubation, the significant proportions of both 4T1 cells and A549 cells exhibited red fluorescence, indicative of DiI-PGEVs. The internalization efficiency of PGEVs was further quantified using flow cytometry. Figure 2G-I also confirmed that the internalization efficiency of DiI-PGEVs by 4T1 and A549 cells improved with increasing incubation time. After 6 h of incubation, the percentages of DiI-PGEVs taken up by 4T1 and A549 cells were 72.2% and 81.3%, respectively. Previous research has indicated

that the efficiency of nanoparticle uptake is influenced by the presence of specific cell surface receptors [38]. Therefore, the difference in the uptake efficiency of PGEVs between 4T1 cells and A549 cells may be attributed to their heterogeneous surface compositions. Furthermore, Raw 264.7 macrophages were also treated with DiI-PGEVs for varying durations. The results (Fig. S4) demonstrated the efficient uptake of DiI-PGEVs by Raw 264.7 cells, with preferential localization in the cytomembrane.

Anti-tumor activity of PGEVs in vitro

The anti-tumor activity of PGEVs in vitro was determined through the CCK-8 assay. As demonstrated in

Fig. 3A and B, PGEVs inhibited the 4T1 and A549 cell proliferation in both concentration- and time-dependent manners, with notable inhibitory effects at 50 µg/mL and 100 µg/mL. After 48 h co-incubation, the viabilities of 4T1 cells were 55.2% and 45.6% for PGEVs at 50 µg/mL and 100 µg/mL, and the viabilities of A549 cells were

73.0% and 60.2% for PGEVs at 50 µg/mL and 100 µg/mL. The data indicated that the PGEVs possessed a greater capacity to suppress the proliferation of 4T1 cells (a TNBC cell line) than A549 cells (a lung cancer cell line). Furthermore, we conducted CCK-8 experiments to evaluate the effect of PD on the survival rates of 4T1 cells and

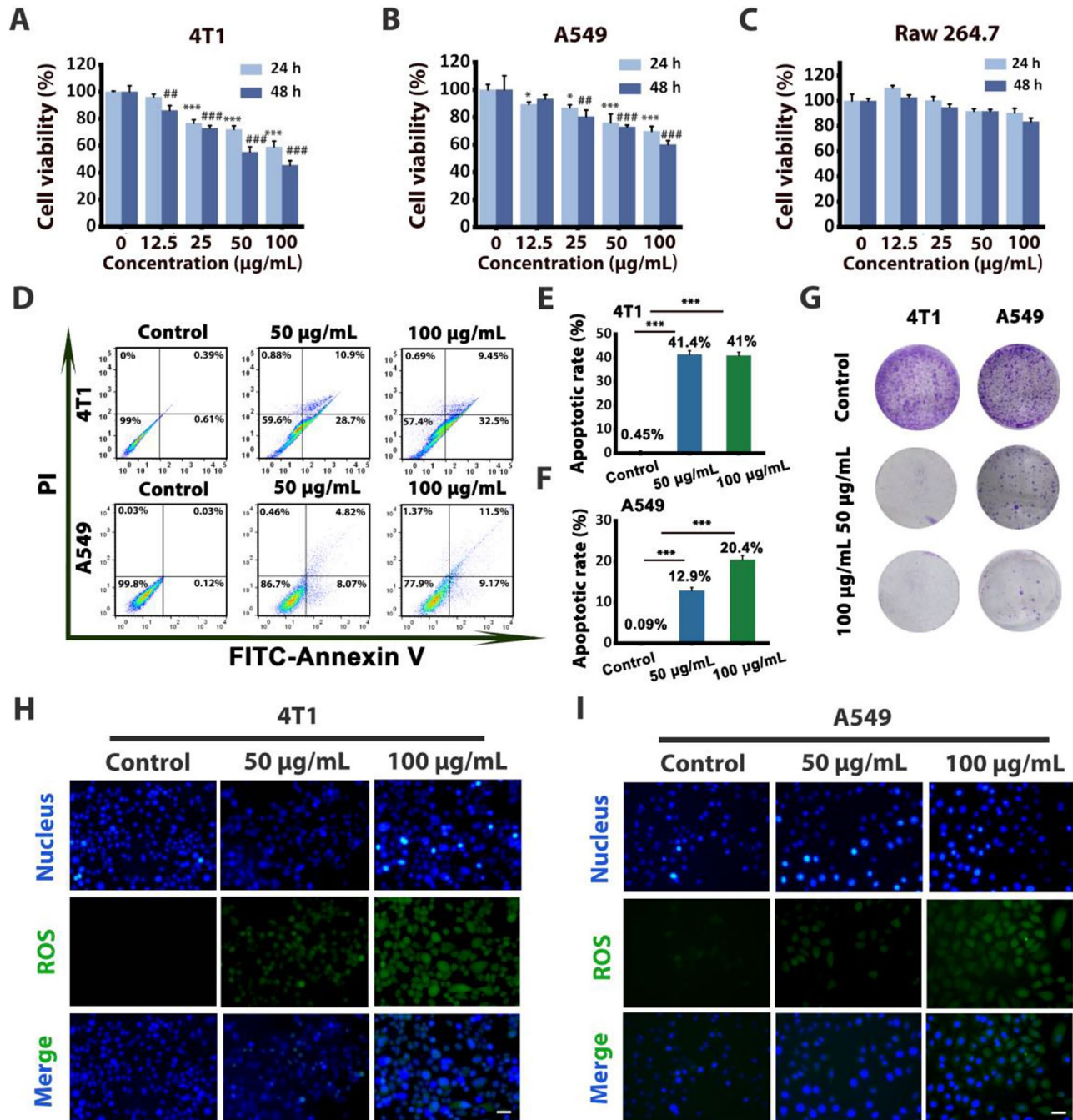


Fig. 3 Anti-tumor activity of PGEVs in vitro. Cytotoxicity of PGEVs in 4T1 cells (A), A549 cells (B) and Raw 264.7 cells (C) post administration of PGEVs at concentrations ranging from 12.5 µg/mL to 100 µg/mL for 24 h and 48 h. **p* < 0.05, ****p* < 0.001 vs. control group (24 h), ##*p* < 0.01, ###*p* < 0.001 vs. control group (48 h). (D) Apoptosis of 4T1 cells and A549 cells after treated with PGEVs at 50 µg/mL and 100 µg/mL for 48 h, as detected by flow cytometry and (E, F) the corresponding quantitative analysis. (G) Plate colony formation of 4T1 cells and A549 cells after treatment with PGEVs. Fluorescence images of 4T1 cells (H) and A549 cells (I) stained with DCFH-DA after treated with 50 µg/mL and 100 µg/mL PGEVs for 48 h, scale bar: 50 µm

A549 cells to compare the efficacy of PGEVs with that of free PD. The results indicated that the PD concentration of 24.6 $\mu\text{g}/\text{mL}$ was necessary to achieve a survival rate of roughly 50% for 4T1 cells and 60% for A549 cells (Fig. S5). Notably, the PD concentration in 100 $\mu\text{g}/\text{mL}$ of PGEVs was a mere 0.342 $\mu\text{g}/\text{mL}$, which suggest that the effect of free PD at 24.6 $\mu\text{g}/\text{mL}$ was comparable to that of PGEVs containing only 0.342 $\mu\text{g}/\text{mL}$ PD. Additionally, we tested the effect of PGEVs on Raw 264.7 cells using CCK-8 assay, which indicated that slight cytotoxicity was detected in Raw 264.7 macrophages even at 100 $\mu\text{g}/\text{mL}$ of PGEVs. Notably, PGEVs exerted slight promotion effect on Raw 264.7 macrophages at a low concentration of 12.5 $\mu\text{g}/\text{mL}$, indicating their potential beneficial effects and excellent biocompatibility (Fig. 3C).

To assess the pro-apoptotic potential of PGEVs on tumor cells, we conducted apoptosis assay by flow cytometry. As indicated in Fig. 3D-F, there was very few apoptotic cells in the control groups without PGEVs treatment. In contrast, after co-culture with PGEVs for 48 h, significantly increased percentages of apoptotic cells were observed in both 4T1 and A549 cells, especially 4T1 cells. The proportion of apoptotic cells, encompassing both early and late stages of apoptosis, was 41% in 4T1 cells and 20.4% in A549 cells. Furthermore, the apoptosis rate of Raw 264.7 cells treated with PGEVs was comparatively low, as illustrated in Fig. S6. The plate colony formation assay is an effective method for evaluating cell proliferation ability. Therefore, we further validated the inhibitory effect of PGEVs on 4T1 cells and A549 cells using clone formation assay. As depicted in Fig. 3G, treatment with PGEVs at 50 $\mu\text{g}/\text{mL}$ and 100 $\mu\text{g}/\text{mL}$ led to obviously fewer colonies formed by both 4T1 and A549 cells compared to untreated cells.

It is generally believed that high level of oxidative stress can induce cytotoxicity and apoptosis in tumor cells [39]. To investigate the mechanisms driving the pro-apoptotic effect of PGEVs on tumor cells, we measured the levels of intracellular ROS in 4T1 and A549 cells following PGEV treatment utilizing the DCFH-DA probe. As shown in Fig. 3H and I, treatment with PGEVs led to a marked increase in ROS levels in both 4T1 and A549 cells. The fluorescence signals from DCF were predominantly localized within the cells and exhibited a concentration-dependent enhancement in intensity. The elevated intracellular ROS production induced by PGEVs treatment may disrupt essential cellular substances involved in tumor cell metabolism, ultimately triggering apoptosis. Furthermore, we performed ROS quantitative analysis by detecting DCF fluorescence intensity of the stained cells with a microplate reader. The results displayed that the ROS levels in PGEVs-administrated 4T1 cells and A549 cells were 12.0-fold and 8.9-fold higher than those in their respective control cells (Fig. S7), which further

indicated that PGEVs treatment significantly promoted oxidative stress in cancer cells. Notably, greater accumulation of ROS was observed in PGEVs-treated 4T1 cells than in A549 cells. This differential ROS response could be a critical factor contributing to the lower viability and higher apoptosis rate observed in 4T1 cells than in A549 cells upon PGEVs treatment.

TAMs polarization induced by PGEVs in vitro

Recently, researchers have increasingly focused on TAMs to rebuild the immunosuppressive TME, thereby enhancing the immunotherapy efficiency of TNBC. TAMs can be classified into tumoricidal M1-TAMs and protumoral M2-TAMs [40]. During the initial stage of tumorigenesis, M1-TAMs are the dominant phenotype and mainly responsible for killing tumor cells. However, as tumors progress, the cytokines released from tumor cells promote the transition of M1-TAMs to M2-TAMs, which facilitate tumor growth and angiogenesis. M2-TAMs are prevalent in a majority of solid tumors and contribute significantly to the immunosuppressive environment within the TME [41]. Therefore, reprogramming TAMs from protumoral M2-TAMs to tumoricidal M1-TAMs offers a promising strategy to reverse the immunosuppressive TME and increase the effectiveness of TNBC therapy. In this study, we employed a transwell co-culture system to simulate TAMs and assess the macrophage reprogramming effect of PGEVs in vitro. In detail, PGEVs treated Raw 264.7 cells were seeded in the upper chamber and co-cultured with 4T1 or A549 cells in the lower chamber. Total RNA was extracted from Raw 264.7 cells, and qRT-PCR experiment was proceeded to detect the gene expressions of M1 markers (iNOS, TNF- α , IL-6 and IL-12) and M2 marker (CD206). The data revealed that treatment with PGEVs significantly upgraded the expressions of iNOS, TNF- α , IL-6 and IL-12 (Fig. 4A-D) and downgraded the expression of CD206 (Fig. 4E). Concretely, in the 4T1/Raw 264.7 co-culture system, PGEVs (50 $\mu\text{g}/\text{mL}$) significantly enhanced the expression levels of iNOS, TNF- α , IL-6 and IL-12 by 46.2, 13.8, 28.7 and 4.9 times and decreased the expression of CD206 by 0.45 times in comparison to the control group group. Similarly, in the A549/Raw 264.7 co-culture system, PGEVs at the same concentration led to 21.1-fold, 4.1-fold, 51.1-fold and 5.2-fold changes in the expression levels of iNOS, TNF- α , IL-6 and IL-12, and 0.68-fold change in the expression level of CD206, compared with those in the control group. Moreover, the concentrations of the typical pro-inflammatory cytokines TNF- α and IL-6 and the anti-inflammatory cytokines IL-4 and IL-10 in the co-cultured Raw 264.7 cell supernatant were tested through ELISA kits. The results displayed that the concentrations of TNF- α and IL-6 were remarkably increased following treatment with PGEVs at 50 $\mu\text{g}/\text{mL}$ in both 4T1/

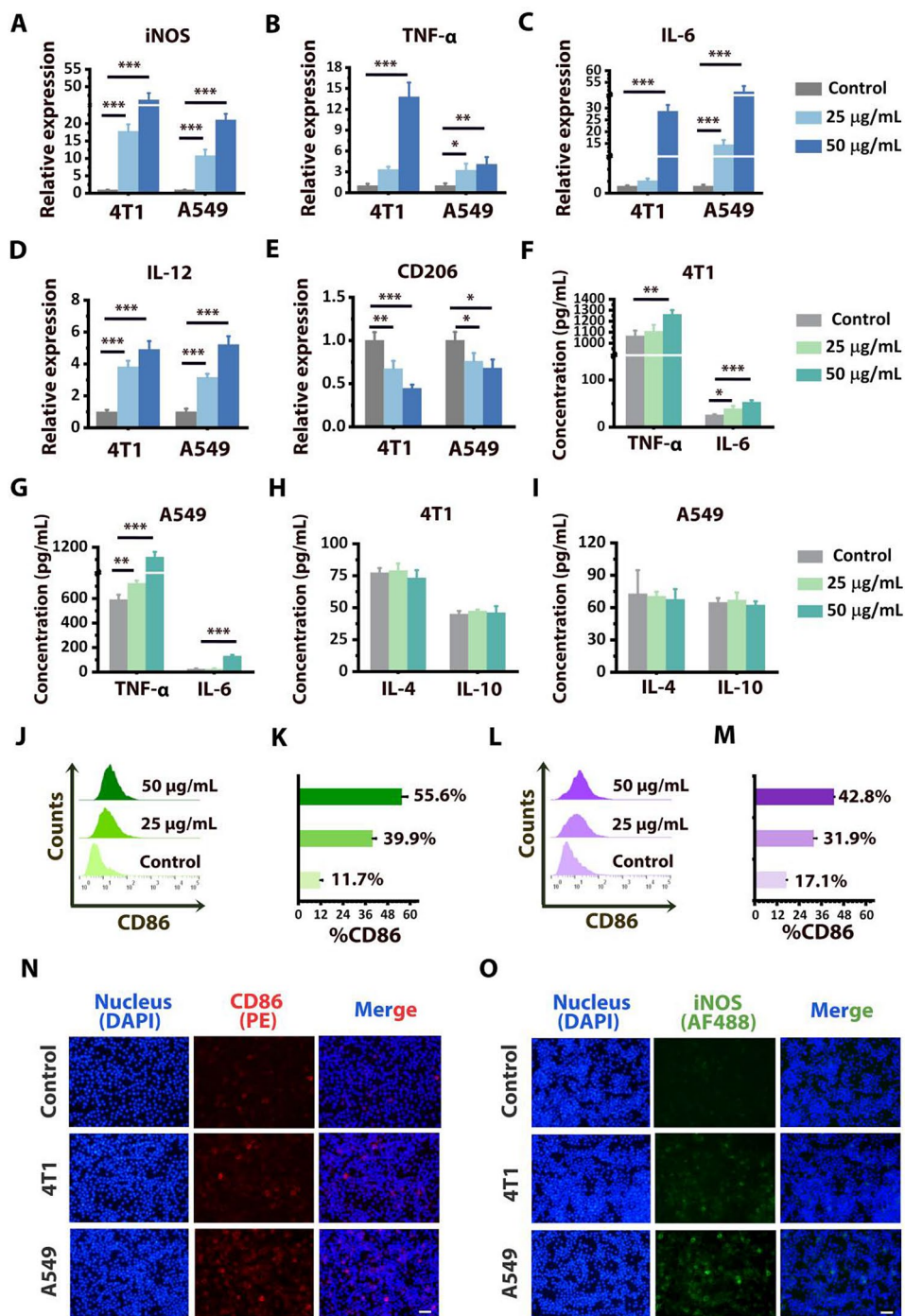


Fig. 4 Polarization of TAMs induced by PGEVs in vitro. The mRNA expression levels of the M1 markers iNOS (A), TNF- α (B), IL-6 (C) and IL-12 (D) and M2 marker CD206 (E) in PGEVs treated Raw 264.7 cells co-cultured with 4T1 cells or A549 cells were evaluated by qRT-PCR, these mRNA expressions were normalized to those of GAPDH. Pro-inflammatory cytokines TNF- α and IL-6 released from PGEVs treated Raw 264.7 cells co-cultured with 4T1 cells (F) and A549 cells (G) were detected by ELISA. Anti-inflammatory cytokines IL-4 and IL-10 released from PGEVs treated Raw 264.7 cells co-cultured with 4T1 cells (H) and A549 cells (I) were detected by ELISA. Representative flow cytometry plots and percentages of CD86⁺ cells (M1 marker) of PGEVs treated Raw 264.7 cells co-cultured with 4T1 cells (J, K) and A549 cells (L, M). Immunofluorescence staining for the M1 marker proteins CD86 (N) and iNOS (O) in PGEVs-treated Raw 264.7 cells co-cultured with 4T1 cells or A549 cells, scale bar: 100 μm

A549 and Raw 264.7 cell co-culture systems (Fig. 4F and G). However, no significant difference was observed in the concentrations of IL-4 and IL-10 (Fig. 4H and I). The above findings collectively indicated that PGEVs treatment effectively promoted the polarization of TAMs toward M1 phenotype.

Next, the Raw 264.7 cells in the transwell system were labeled with the M1 marker protein CD86, and the percentage of CD86⁺ macrophages was quantitatively measured using flow cytometry to assess the effect of PGEVs on macrophage phenotypic conversion. As indicated in Fig. 4J–M, Raw 264.7 cells were polarized by PGEVs, resulting in CD86⁺ percentage of 55.6% in the 4T1/Raw 264.7 system and 42.8% in the A549/Raw 264.7 system. To further verify the effect of PGEVs on macrophage polarization, we determined the expression of the M1 marker proteins CD86 and iNOS in Raw 264.7 cells by immunofluorescence staining. As shown in Fig. 4N and O, compared with control group, PGEVs treatment resulted in greater fluorescence intensities of CD86 and iNOS in Raw 264.7 cells, which was consistent with the results from flow cytometry. These findings illustrated that PGEVs treatment could polarize TAMs to M1 phenotype in the microenvironments of both 4T1 and A549 cells.

It is generally believed that the release of pro-inflammatory cytokines such as TNF- α , IL-6 and IL-12 from polarized macrophages can induce cancer cell death. Herein, we evaluated the viability of cancer cells in the lower chamber through CCK-8 assay. As indicated in Fig. S8, PGEVs treatment clearly inhibited the proliferation of both 4T1 and A549 cells. In comparison to the control group, the viability of 4T1 cells decreased to 41.1% at PGEVs concentration of 50 μ g/mL, while the viability of the A549 cells was 54.8% at the same PGEVs concentration. The above results indicated that polarized TAMs by PGEVs can suppress cancer cell growth, particularly in the TNBC cell line 4T1.

Biodistribution of PGEVs in vivo

In clinical cancer treatment, i.v. injection is a commonly used technique that delivers drugs directly into the bloodstream, allowing for swift onset of their effects. On the other hand, oral administration ensures stable absorption via the gastrointestinal tract and maintains a relatively sustained blood concentration. It is cost-effective, as it does not require specialized infusion sets or medical personnel involvement, offering a higher psychological acceptance in patients. Since these two methods possess their own advantages, we comparatively assessed the in vivo biodistribution of PGEVs through both oral administration and i.v. injection. The PGEVs labeled with fluorescent dye DiD (DiD-PGEVs) were orally or i.v. administered to the mice. Mice given PBS served as

control group. The DiD fluorescence signals from the mice were tracked at different intervals and observed through an animal in vivo imaging system.

Figure 5A exhibited that substantial DiD fluorescence was predominantly detected at the abdominal regions of the mice in both oral and i.v. administration groups and steadily enhanced within 3 h, with the mice in the i.v. administration group exhibiting stronger fluorescence (Fig. 5B). Then the signals in abdominal regions gradually weakened after 6 h of administration and were barely observed by 48 h in the oral treatment group. However, strong signals persisted intensely in i.v. injection group even after injection for 48 h. At the designated time, the mice were executed, and their main organs, brains and intestines were harvested for fluorescence observation. The majority of the fluorescence from DiD-PGEVs was detected in the livers and kidneys of both orally and i.v. treated mice (Fig. 5C–F). Compared with those in the livers and kidneys, the fluorescence signals in the lungs were much weaker in both PGEVs treatment groups (Fig. S9). There were negligible accumulation of DiD-PGEVs in the hearts and spleens at any time points, as very little fluorescence was detected in these organs from both groups. Notably, DiD-PGEVs rapidly accumulated in the brain after both administration methods. Within 1 h of oral and i.v. administration, the DiD-PGEVs effectively traversed the blood-brain barrier (BBB) and successfully targeted brain regions. The strongest fluorescence intensity at the brain sites occurred at 12 h after both oral and i.v. treatment. In particular, in the i.v. injection group, the signal in the brain persisted even at 48 h post-administration. The above observations suggest that once entering the circulatory system in vivo, DiD-PGEVs can be quickly captured primarily by the liver and kidney and demonstrated a robust capacity to penetrate the BBB. Additionally, following oral administration, sustained and intense DiD fluorescence signals were observed in the intestinal tract of the mice and gradually faded after 24 h (Fig. 5G and Fig. S10). In the i.v. injection group, the fluorescence signal of DiD-PGEVs was relatively weaker than that in the oral group and tended to attenuate after 12 h of injection. Minimal signals may originate from food residues within the gastrointestinal tract in PBS group. Therefore, we verified that PGEVs can remain stable in gastric and intestinal fluids and exhibit gastrointestinal absorption characteristics in vivo.

In summary, the biodistribution of PGEVs in vivo differed between the oral and i.v. administration routes. The data indicated that the majority of the PGEVs were absorbed by the liver and kidney and could cross the BBB to reach brain sites. They could persist in the GIT, thereby allowing the encapsulated contents to cross the intestinal barrier and enter the circulatory system effectively.

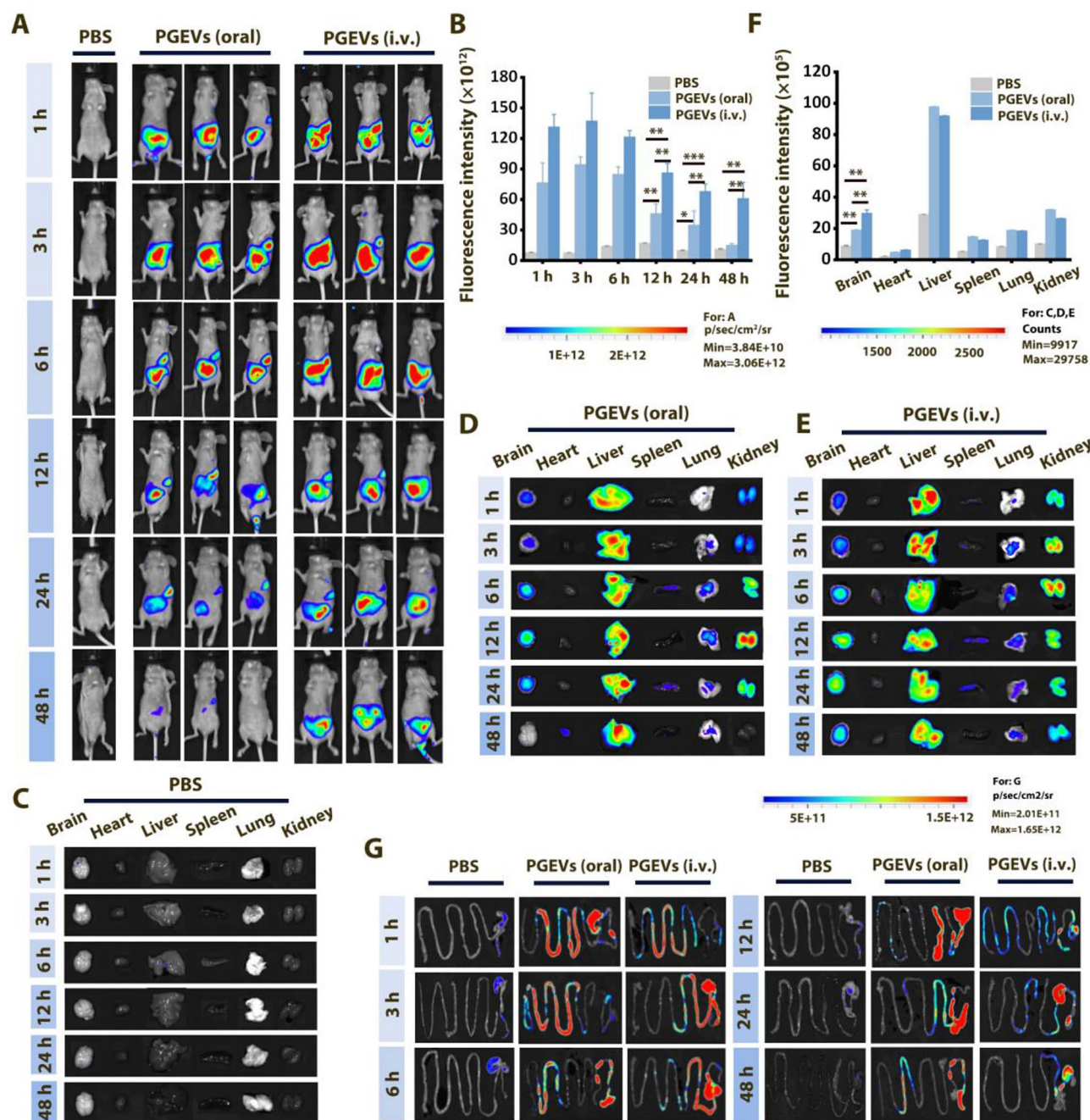


Fig. 5 The biodistribution of PGEVs in vivo. **(A)** Biodistribution of PBS, PGEVs (oral) and PGEVs (i.v.) in mice after treatment for 1 h, 3 h, 6 h, 12 h, 24 h and 48 h. **(B)** The quantitative results of the mice in different treatment groups. Biodistribution of PBS **(C)**, PGEVs (oral) **(D)** and PGEVs (i.v.) **(E)** in main organs from different treatment groups. **(F)** The quantitative results of the main organs from different treated mice after 24 h. **(G)** Biodistribution of PBS, PGEVs (oral) and PGEVs (i.v.) in intestinal tract

Biosafety in vivo

In the biosafety evaluation system of nanodrugs, monitoring the impact of drugs on the body weight of mice initially provides insights into potential adverse effects. If a drug is highly toxic, significant changes in mouse body weight may occur following administration. Herein, the body weights of the mice after oral administration

and i.v. injection of PGEVs were recorded to assess their biosafety. As depicted in Fig. S11, oral or i.v. injection of PGEVs at different doses did not significantly affect the body weights of the mice, closely resembling the trends observed in the control group. The liver and kidneys are essential organs that participate in the immune response, metabolism and detoxification within the body.

Drugs and their metabolites can potentially impose burdens and even induce toxicity on these organs. Clinical research indicates that drugs with potential toxicity to the liver and kidney significantly constrain their widespread application. AST and ALT are crucial enzymes that are primarily concentrated in the liver. Abnormal serum levels of these enzymes indicate liver injury. BUN and CREA are the final metabolites of protein and nitrogenous organic matter, which are excreted through the kidneys. Elevated or decreased levels of these substances indicate kidney damage or dysfunction. The above indices, including ALT, AST, BUN and CREA, are commonly utilized in clinical settings for the evaluation of hepatorenal toxicity. Our study revealed that continuous oral and i.v. administration of PGEVs, even at high concentration did not significantly affect any of these four indicators in comparison to the control group (Fig. 6A-D). Moreover, we performed histological evaluations using H&E staining to assess the impacts of PGEVs on five main organs (heart, liver, spleen, lung and kidney) and the brain. As

presented in Fig. 6E, no morphological abnormalities or tissue damage were observed in these organs and brains following oral or i.v. administration of PGEVs at different concentrations. These findings further underscore the favorable biosafety profile of PGEVs.

In vivo anti-tumor efficiency of PGEVs

Encouraged by the superior results in vitro, we investigated the anti-tumor effect and mechanism of PGEVs against TNBC in vivo in a subcutaneous xenograft TNBC mouse model. Prior to evaluating the anti-tumor efficiency of PGEVs, the tumor accumulation of PGEVs were assessed in tumor-bearing mice. PGEVs were labeled with the fluorescence dye DiD and orally given or i.v. injected into the tumor-bearing mice. Then, the mice were executed at different intervals, and the main organs and tumors were imaged with an animal in vivo imaging system. As illustrated in Fig. 7A, DiD-PGEVs gradually accumulated at tumor sites regardless of the two different drug administration methods. The fluorescence

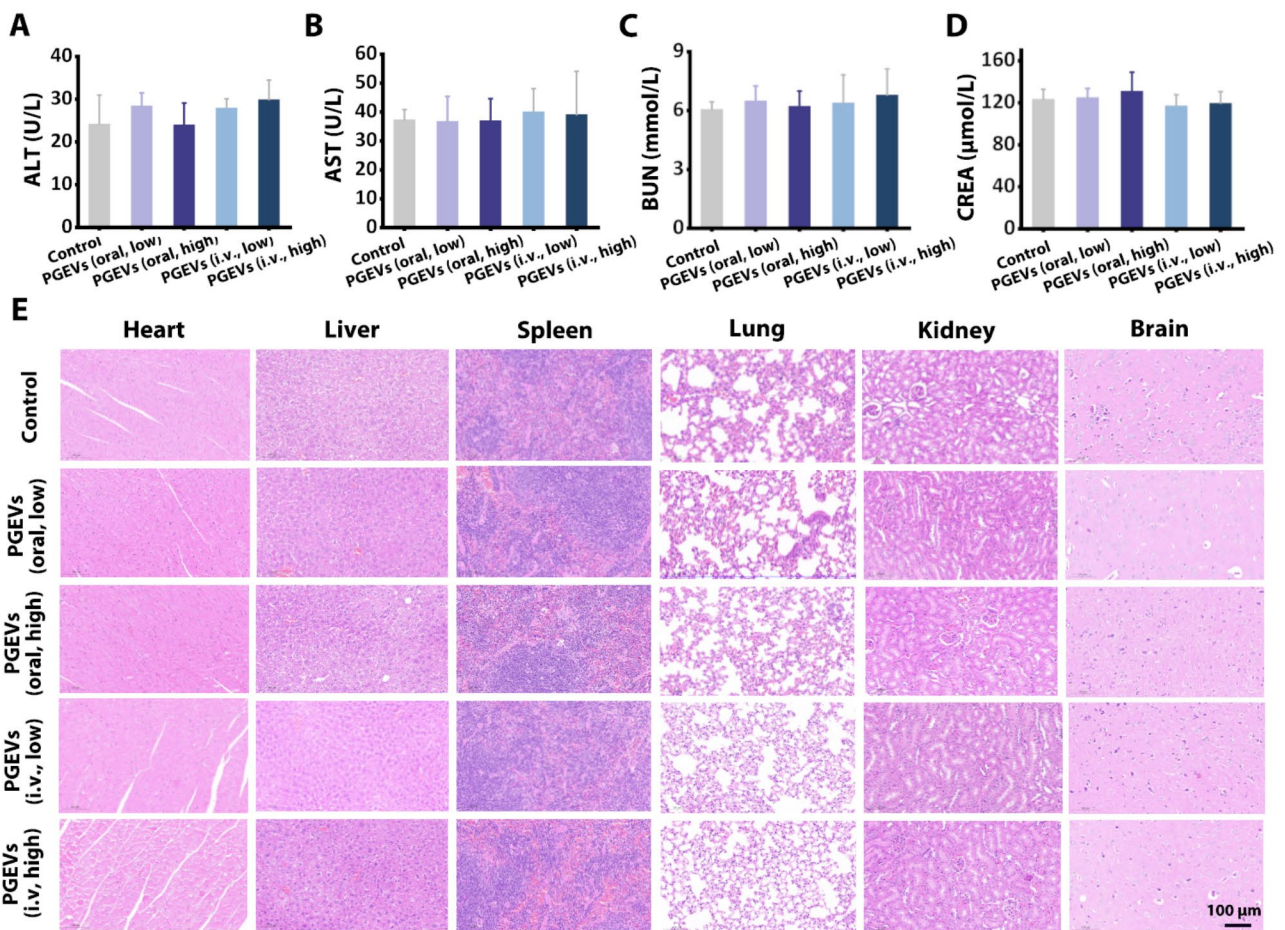


Fig. 6 Biosafety of PGEVs in vivo. ALT (A), AST (B), BUN (C) and CREA (D) concentrations in the serum of the mice after oral administration and i.v. treatment. (E) H&E staining image of five main organs and brains in different treatment groups, scale bar: 100 μm

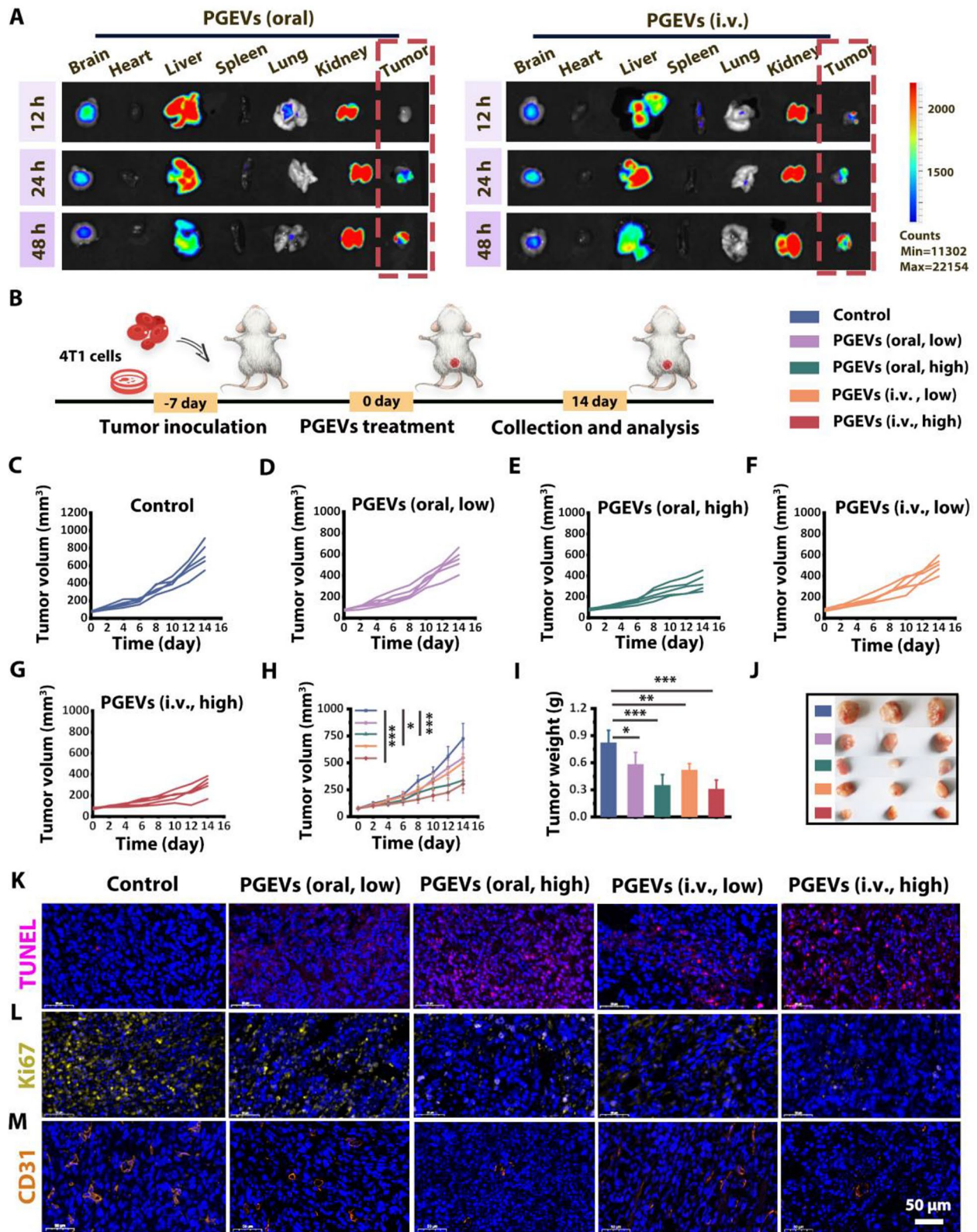


Fig. 7 Anti-tumor efficacy of PGEVs in vivo. **(A)** Biodistribution of DID-PGEVs in main organs and tumors after oral administration and i.v. injection for 12 h, 24 h and 48 h in tumor-bearing mice. **(B)** Schematic illustration of the anti-tumor experimental protocol. **(C-G)** Individual tumor sizes of control, PGEVs (oral, low), PGEVs (oral, high), PGEVs (i.v., low) and PGEVs (i.v., high)-treated mice. Average tumor growth curves **(H)**, tumor weights **(I)**, and representative tumor images **(J)** in the different treatment groups. Representative images of tumor sections after immunofluorescence staining with TUNEL **(K)**, Ki67 **(L)** and CD31 **(M)**

signals from DiD-PGEVs increased steadily at tumor sites 24 h after oral administration and 12 h after i.v. injection. Notably, the strongest fluorescence signal in the tumors was observed after 48 h of administration via both the oral and i.v. routes. Furthermore, intense fluorescence signals were detected in the livers, kidneys and brains for both administration methods, and a considerable intensity maintained for 48 h.

For investigating the therapeutic effect of PGEVs, the mice with TNBC tumors were treated with the control, PGEVs (oral, low), PGEVs (oral, high), PGEVs (i.v., low) or PGEVs (i.v., high) every two days (Fig. 7B). The tumor volumes and body weights of the different treated mice were measured every two days. Figure 7C-G illustrated the changes in the tumor volumes of the mice in the different groups. The tumors in the control group rapidly progressed, whereas all PGEVs treatments effectively inhibited tumor growth to varying degrees. Compared with those in the control group, the average tumor volumes at the end of the different treatments (Fig. 7H) were 1.33-, 2.14-, 1.44- and 2.39-fold smaller in PGEVs (oral, low), PGEVs (oral, high), PGEVs (i.v., low) and PGEVs (i.v., high) groups, respectively. Notably, although the PGEVs (i.v., high) treatment resulted in a greater tumor inhibition rate than that of PGEVs (oral, high) treatment, there was no significant difference between the two groups. The mean tumor weights in both PGEVs (oral, high) group and PGEVs (i.v., high) group were lower than those in the other groups (Fig. 7I). Additionally, the alterations in tumor sizes (Fig. 7J) aligned with the changes observed in both tumor volumes and weights. The body weights of the mice remained relatively stable across the five groups (Fig. S12). Furthermore, TUNEL staining and Ki67 immunofluorescence staining were proceeded to assess the pro-apoptotic and proliferation-inhibitory effects of PGEVs on tumors in vivo. Compared to the PGEVs (oral, low) and PGEVs (i.v., low) groups, the PGEVs (oral, high) and PGEVs (i.v., high) groups exhibited higher red fluorescence of TUNEL, indicating their strong pro-apoptotic effects on TNBC (Fig. 7K). The expression level of Ki67 represents the degree of cell proliferation. A high level of Ki67 expression indicates a high rate of tumor proliferation and aggressiveness. In comparison to the control group, different degrees of Ki67 fluorescence (yellow) were detected in all PGEVs treatment groups, with the weakest signals observed in the PGEVs (oral, high) and PGEVs (i.v., high) groups, suggesting the marked decrease in the number of proliferative cells in these groups (Fig. 7L). Additionally, the antiangiogenic activity of PGEVs was assessed via CD31 (angiogenesis marker) immunofluorescence staining. As demonstrated in Fig. 7M, the expression levels of CD31 (orange fluorescence) in the PGEVs (oral, high) and PGEVs (i.v., high) groups were significantly lower

compared with those in the control, PGEVs (oral, low) and PGEVs (i.v., low) groups, which demonstrated a significant reduction in CD31⁺ blood vessels associated with tumors and underscored the angiogenesis inhibition capacity of PGEVs. Collectively, the above results confirmed the effective therapeutic effect of PGEVs on TNBC tumors in vivo regardless of the oral or i.v. route of administration.

Systemic immune response induced by PGEVs in vivo

We aimed to further understand the mechanisms underlying the highly successful TNBC treatment outcomes of PGEVs. Herein, the immune cells within tumors were analyzed to evaluate the regulatory impact of PGEVs on the TME in vivo. Firstly, at the end of the treatments, tumors from the various groups were harvested, and flow cytometry was used to analyze the proportions of M1-TAMs and cytotoxic T lymphocytes (CTLs) within the tumors. Antibodies against F4/80 and CD86 were used to label M1 macrophages. Compared with the control group, we found varying increases in the proportions of CD86⁺F4/80⁺ cells in all PGEVs treatment groups. Treatment with PGEVs (oral, high) significantly elevated the percentage of CD86⁺F4/80⁺ cells to 22.5%, a level comparable to that observed in PGEVs (i.v., high) treatment group (26.1%) (Fig. 8A and Fig. S13). The results revealed that PGEVs promoted the reprogramming of TAMs to M1 type. CTLs contribute to anti-tumor immunity by directly killing tumor cells or by regulating the activity of other immune cells. Flow cytometry was used to measure the percentage of CD3⁺CD8⁺ cells, which reflects the infiltration of CTLs in the tumors. As presented in Fig. 8B and Fig. S14, the percentages of CD3⁺CD8⁺ cells in tumors were markedly increased following treatments with PGEVs (oral, high, 21.8%), PGEVs (i.v., low, 16.2%) and PGEVs (i.v., high, 24.5%), whereas such infiltration was largely absent in mice subjected to control (1.12%) or PGEVs (oral, low, 3.33%) group. We then assessed the expressions of the cytotoxic factors IFN- γ and Granzyme B (GzMB) in tumor, which contribute to promote the activation and enhance the killing function against tumor cells of CTLs. Compared with those in the control group, both PGEVs (oral, high) and PGEVs (i.v., high) significantly increased the expression levels of these factors (Fig. 8C and D), suggesting that PGEVs enhanced the cytotoxicity of CTLs against tumors. Furthermore, we explored the mechanism through which PGEVs boosted the cytotoxic activity of CTLs. We measured the protein expression of PD-1 on the tumor tissues after different treatments through immunofluorescence staining. PD-1 is an immune checkpoint protein that is expressed primarily on T cells. By exploiting PD-1 signaling, tumors induce exhaustion or dysfunction of T cells to evade immune surveillance and

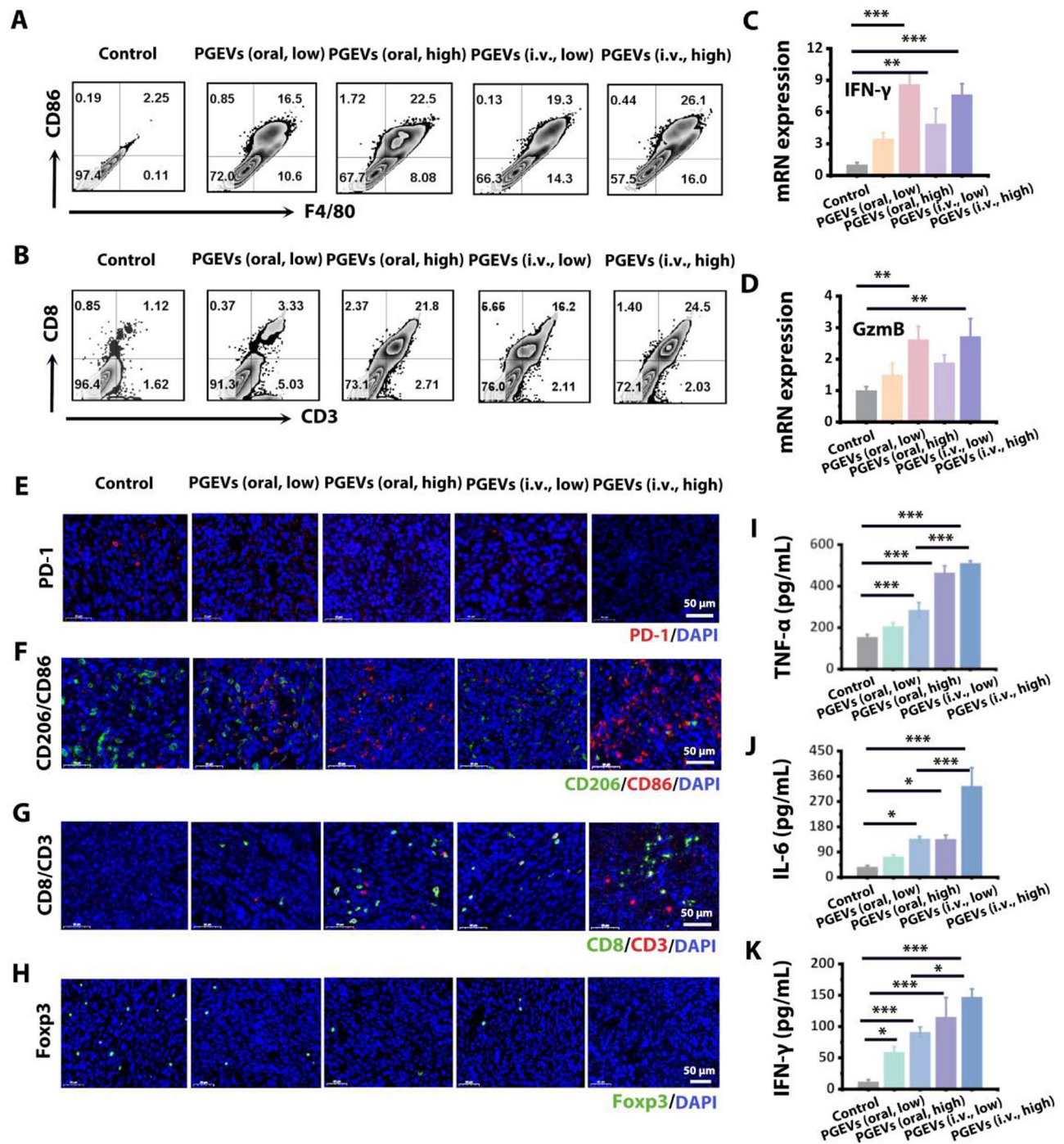


Fig. 8 In vivo immune response evaluation. Representative flow cytometry plots of CD86⁺F4/80⁺ cells (A) and CD3⁺CD8⁺ cells (B) in tumors from mice after treatment with Control, PGEVs (oral, low), PGEVs (oral, high), PGEVs (i.v., low) and PGEVs (i.v., high). qRT-PCR analysis of the relative mRNA expression levels of IFN- γ (C) and GzmB (D) in tumors after different treatments. (E) Immunofluorescence staining images of PD-1⁺ cells in tumors from mice after different treatments. Immunofluorescence staining images of CD206⁺CD86⁺ (F), CD3⁺CD8⁺ (G) and Foxp3⁺ (H) cells in tumors from the mice after different treatments. Cytokine levels of TNF- α (I), IL-6 (J) and IFN- γ (K) in the serum of mice from different groups

grow uncontrollably, thus promoting tumor progression [42]. The immunofluorescence staining results clearly demonstrated that both orally and i.v treated PGEVs reduced the expression of PD-1 on tumors, (Fig. 8E),

which may be responsible for the enhanced cytotoxicity of CTLs against tumor cells.

To further clarify the regulatory effect of PGEVs on the TME at the tissue level, tumor tissues were collected, and

an immunofluorescence staining experiment was performed to assess the immune response *in vivo*. The results of immunofluorescence staining for CD86 (M1-TAMs marker) and CD206 (M2-TAMs marker) (Fig. 8F and Fig. S15) clearly demonstrated that M2-TAMs were dominant in the control group since they presented the strongest green fluorescence from CD206 and the lowest red fluorescence from CD86. In the PGEVs (oral, high) and PGEVs (i.v., high) groups, the green fluorescence intensity diminished while the red fluorescence intensity increased, suggesting that PGEVs treatment effectively promoted the polarization of TAMs to the M1 phenotype. CTLs are known for their ability to kill tumor cells. As depicted in Fig. 8G and Fig. S16, the results of immunofluorescence staining for CD3 and CD8 demonstrated that the PGEVs (oral, high) and PGEVs (i.v., high) groups exhibited the highest abundance of CD3⁺ and CD8⁺ cells. The elevated infiltration of CD3⁺/CD8⁺ T cells is important for restraining tumor growth in mice. Foxp3 is widely recognized as the most specific marker for Tregs, which are pivotal target for therapeutic intervention due to their capability to suppress T cell proliferation and effector cytokines production. Consequently, evaluating the expression of Foxp3 within tumors offers important insights into tumor progression and prognosis. Additionally, we conducted immunofluorescence staining experiment to assess the expression of Foxp3. In Fig. 8H, the expression of Foxp3 reduced after PGEVs (oral, high) and PGEVs (i.v., high) treatments compared to the control group, whereas no significant changes were detected in the PGEVs (oral, low) and PGEVs (i.v., low) groups.

Cytokines are critical for activating and regulating the immune response. Changes in the host immune status lead to corresponding alterations in the levels of cytokines *in vivo*. Herein, we detected the levels of cytokines (TNF- α , IL-6 and IFN- γ) associated with anti-tumor immune responses in mouse serum via ELISA assay. TNF- α and IL-6 are essential mediators that activate innate immune cells, IFN- γ is responsible for inducing adaptive cell-mediated immunity, which are crucial for a robust immune response in tumor immunotherapy. The concentrations of TNF- α , IL-6 and IFN- γ in mice serum clearly increased following PGEVs (i.v., low) and PGEVs (i.v., high) treatments (Fig. 8I-K). Although PGEVs (oral, low) and PGEVs (oral, high) administration also led to elevated cytokine concentrations of TNF- α , IL-6 and IFN- γ , they were lower than those observed in PGEVs (i.v., high) group. This was probably because the effects of oral administration and *i.v.* injection differ significantly in terms of drug absorption, distribution, and metabolism. *I.v.* administration allows drugs to bypass the digestive absorption process and enter directly into the bloodstream. In contrast, oral administration requires drug absorption through the GIT, drugs interact with the gut

microbiota, potentially altering their composition and functionality.

Modulation of the gut microbiota by PGEVs

Research on the gut microbiota is becoming increasingly vital in personalized tumor treatment [43]. Understanding the individual's gut microbiota could optimize drug treatment strategies, minimize side effects, and enhance tumor therapeutic outcomes. The gut microbiota constitutes a complex ecosystem within the GIT, and increasing evidence indicates that the gut microbiota is highly associated with the initiation, progression, and therapeutic response of various tumors, including TNBC [44]. Dysbiosis refers to changes in the diversity and composition of the gut microbiota, which may compromise the integrity of the intestinal barrier, potentially resulting in increased intestinal permeability and the translocation of pathogenic bacteria. In our work, we conducted 16S rRNA gene sequencing to comparatively analyze the microbial compositions of feces from mice in different groups. Alpha diversity (Chao1, Shannon and Simpson indices) reflects the species abundance and diversity of the gut microbiota. A higher Chao1 index indicates increased flora abundance, and higher Shannon and Simpson indices indicate increased flora diversity. Augmenting the abundance and diversity of the gut microbiota in mice is beneficial for impeding tumor development. As depicted in Fig. 9A-C, compared to the healthy control group, the Chao1, Simpson and Shannon indices were lower in the tumor control group. Following PGEVs (oral, high) and PGEVs (i.v., high) treatment, Chao1, Simpson and Shannon indices increased compared to those of the tumor control group. The Chao1, Simpson, and Shannon indices were greater in the PGEVs (oral, high) group compared to the PGEVs (i.v., high) group. The Venn diagram effectively illustrates the number of shared and unique species, highlighting the similarity and overlap among different groups. The data (Fig. 9D) revealed that PGEVs (oral, high) treatment resulted in a notable increase in operational taxonomic units (OTUs), totaling 2235 strains, comprising 196 strains shared across all groups and 1412 strains unique to this treatment, which was in line with the trend observed in the Chao1, Simpson and Shannon indices. Principal coordinate analysis (PCoA) reveals the similarities in microbiota composition across different groups, with the distance between any two groups reflecting variations along the PCoA axes. The results in Fig. 9E demonstrated that there were certain differences between the tumor control group and the healthy control group.

Furthermore, the composition of gut microbiota at the genus level was analyzed (Fig. 9F). Compared to the healthy control group, the relative abundance of the harmful bacteria *Bacteroides* increased in the tumor

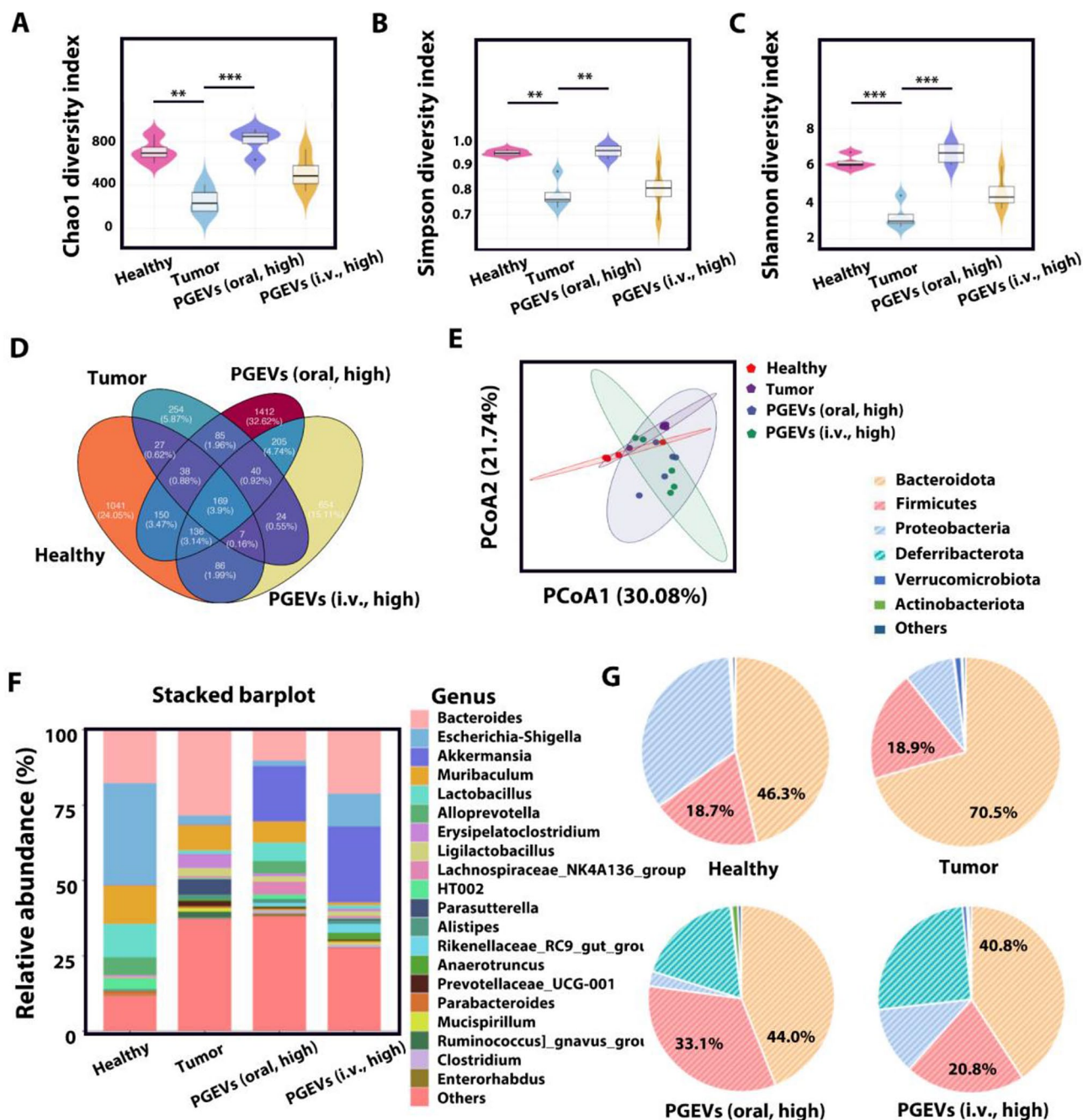


Fig. 9 Gut microbiota modulating effect of PGEVs. Alpha diversity were presented as violin diagrams of the Chao1 (A), Shannon (B) and Simpson (C) indices. (D) Venn diagram of common and unique bacterial species in mice from different treatment groups. (E) PCoA plots of the gut microbiota. The genus (F) and phylum (G) levels of gut microbiota compositions in different treated mice

control group. Following oral or i.v. injection of PGEVs, the relative abundance of *Bacteroides* decreased, and the PGEVs (oral, high) treatment resulted in a much lower relative abundance of *Bacteroides* than that in PGEVs (i.v., high) group. As beneficial bacteria, *Lactobacillus* have been reported to alleviate galactose-induced liver injury through reducing liver inflammation, thus improving the intestinal barrier and regulating microbiome metabolism

[45]. The tumor control group exhibited a lower relative abundance of *Lactobacillus*. In contrast, the PGEVs (oral, high) group presented an increase in *Lactobacillus* abundance, and such phenomenon was inconspicuous in PGEVs (i.v., high) group. Figure 9G presented the gut microbiota composition classified at the phylum level. The dominant phylum of the different treatment groups were *Bacteroidota*, *Firmicutes* and *Proteobacteria*. In

the intestine, *Firmicutes* and *Bacteroidota* are the predominant species of gram-positive and gram-negative bacteria, respectively. Alterations in their ratio indicate gut dysbiosis. Higher *Firmicutes/Bacteroidota* ratio was detected in the PGEVs (oral, high) group and PGEVs (i.v., high) group than in the tumor control group, demonstrating that PGEVs treatment maintained the balance of the gut microbiota. Overall, PGEVs treatment possessed the potential to increase the abundance and diversity of the gut microbiota and correct microbiota disorders, which was beneficial for suppressing tumor development.

Discussion

With the development of nanotechnology, utilizing nanomedicine as efficient agents for the treatment of TNBC represents an optimal approach [46]. Recently, PEVs as natural nanomaterials have emerged as promising therapeutic agents to treat different diseases due to their large-scale production, high bioavailability and high biosafety characteristics [47]. For instance, bitter melon-derived PEVs improved the therapeutic outcome and reduced the drug resistance of 5-fluorouracil in oral squamous cell carcinoma [48]. Momordica charantia-derived PEVs suppressed the proliferation, migration, and invasion of glioma through modulating the PI3K/AKT signaling pathway [49]. PG is a traditional Chinese medicine, which has been reported to possess various pharmacological functions [50]. PD, the main active component of PG, exerts inhibitory effects on a variety of tumors [51] through inhibiting cell proliferation, promoting apoptosis, and antiangiogenesis, and demonstrates potent immunotherapeutic efficacy through immunomodulation. However, the limited solubility and unsatisfied bioavailability (only 1.89%) of PD hindered its clinical application [28]. PEVs, with their unique composition and structure, can encapsulate and protect their contents, breaking the limitations of poor solubility and low bioavailability such as saponins. Moreover, compared with single component, PEVs contain a variety of bioactive ingredients, which can achieve a comprehensive therapeutic effects based on multiple targets and signaling pathways. Herein, we isolated PGEVs from PG and investigated its anti-tumor effect and the underlying mechanism based on regulating immune response and gut microbiota. The current study provides supportive evidences for the potential of PGEVs as a TNBC therapeutic agent.

In this study, we isolated PGEVs from fresh PG through ultracentrifugation and sucrose gradient centrifugation method. Our data showed that PGEVs exhibited spherical structure with a diameter of 73 nm and a zeta potential of -19.23 mV, and contained proteins, lipids, RNAs and active molecules. Phospholipids in PGEVs, including LPC, PE, PG and PC, are crucial in immune

cell regulation, suggesting the potential of PGEVs in immunomodulatory processes (Fig. 1F). In addition, PGEVs exhibited efficient cellular uptake by tumor cells and macrophages in a time-dependent manner, which is crucial for their therapeutic efficacy. After entering the tumor cells, PGEVs displayed significant anti-cancer activity in vitro, particularly against 4T1 cells (a TNBC cell line), by inhibiting tumor cell proliferation and inducing tumor cell apoptosis. ROS plays a critical role in inducing tumor cell apoptosis by activating tumor suppressor proteins and disrupting cellular homeostasis [52, 53]. In previous study, PEVs isolated from lemon juice, could elevate intracellular ROS levels and induce S-phase cell cycle arrest, ultimately resulting in tumor cell apoptosis [54]. Tea flowers-derived PEVs exhibited potent cytotoxic effects on cancer cells by escalating ROS levels, which induced mitochondrial dysfunction and cell cycle arrest, thereby inhibiting the proliferation, invasion and migration of breast cancer cells [18]. Our results displayed that treatment with PGEVs led to a substantial increase in intracellular ROS levels, suggesting a role for oxidative stress in PGEVs-induced tumor cell proliferation inhibition and apoptosis, especially for a TNBC cell line (Fig. 3H and I). Importantly, the anti-tumor effect of free PD at 24.6 $\mu\text{g}/\text{mL}$ is comparable to that of PGEVs containing only 0.342 $\mu\text{g}/\text{mL}$ PD, which indicated that the anti-tumor activity of PGEVs was not solely attributed to their content of PD. Instead, it is likely due to the synergistic outcome of all the bioactive components in PGEVs (proteins, lipids, RNAs, and active substances). Furthermore, the protective nature of their bilayer phospholipid membrane structure, as well as their capability in transmembrane transport and delivery, contribute to the superior anti-tumor activity of PGEVs.

TAMs have gradually become an important protocol and option in TNBC immunotherapy in recent years. M1-TAMs, characterized by their pro-inflammatory properties, are involved in inhibiting tumor proliferation, thus playing a role in anti-tumor responses [55]. Conversely, M2-TAMs, with their anti-inflammatory nature, contribute to tumor promotion, which support tumor growth, proliferation and metastasis [56]. The prevalence of M2-TAMs in solid tumors contributes significantly to the immunosuppressive TME. Thus, strategies that reprogramming TAMs to M1 phenotypes hold promise for countering the immunosuppression in TME and bolstering the effects of TNBC therapy. In our work, we employed a transwell co-culture system to simulate TAMs [57]. The polarization effect of TAMs by PGEVs was assessed after PGEVs treatment (Fig. 4). Our findings demonstrated PGEVs significantly upregulated the expressions of M1 marker proteins and genes (iNOS, CD86, TNF- α , IL-6 and IL-12) and downregulated the expression of M2 marker gene (CD206), indicating a shift

towards the M1 phenotype. Moreover, PGEVs treatment increased the levels of pro-inflammatory cytokines of TNF- α , IL-6 and IL-12, further confirming the M1 polarization effect of PGEVs on TAMs. However, we did not detect notable changes in the release of M2 anti-inflammatory cytokines IL-4 and IL-10. A large number of studies reported that natural products from plant promote the M1 polarization of macrophages. Baicalein have been reported to inhibit breast cancer and melanoma growth by promoting the polarization of TAMs towards M1 phenotype, however, it did not affect the percentage of CD206⁺ M2-TAMs [58]. Astragalus polysaccharide RAP induced M1 phenotype of macrophages, but they could not induce Arg-1 and CD206 expression change [59].

In TNBC mice model, PGEVs administered both orally and intravenously resulted in significant inhibition of tumor growth (Fig. 7). This therapeutic efficacy was confirmed by increased apoptosis (TUNEL staining) and reduced proliferation (Ki67 expression) in TNBC tumors. Angiogenesis marker CD31 significant decreased, demonstrating that PGEVs may disrupt the pro-angiogenic environment, thereby inhibiting tumor growth. Furthermore, we unveiled the mechanisms behind the successful treatment outcomes of PGEVs against TNBC through the modulation of immune cells within the TME (Fig. 8). Treatment with PGEVs significantly enhanced the percentage of M1-TAMs and enhanced the infiltration of CTLs. Additionally, PGEVs treatments decreased PD-1 expression in tumors, boosting the anti-tumor activity of CTLs. The concentrations of cytokines TNF- α , IL-6 and IFN- γ in the serum, which are associated with anti-tumor immune responses, significantly increased after PGEVs treatment. These findings suggest that PGEVs could effectively activate and regulate the immune response and enhance the immunotherapeutic effect of TNBC.

The gut microbiota is gaining growing recognition for its crucial influence on human health and disease. Recent research, spanning from preclinical studies to clinical trials, have progressively confirmed the importance of gut microbiota on anti-tumor effectiveness and immunomodulation [60, 61]. Alpha diversity (Chao1, Shannon and Simpson indices) reflects the abundance and diversity of the gut microbiota. A decrease in the alpha diversity of fecal bacterial composition is linked to reduced survival rates in cancer patients [62]. Patients with a high diversity of gut microbiota exhibit stronger anti-tumor immune responses, which is attributed to an increase in antigen presentation and the improved T cell function [62]. Another study found that patients who had a positive response to PD-1 immunotherapy exhibited greater diversity in their gut microbiota. Compared to those with lower diversity, patients with greater gut microbiota diversity experienced significantly prolonged progression-free survival and showed a greater frequency

of CD8⁺ T cells and NK cells in the peripheral blood [63]. In our study, both the administration of PGEVs orally and i.v. led to a notable enhancement in the abundance and diversity of gut microbiota in TNBC mice, as demonstrated by the elevated Chao1, Simpson, and Shannon indices (Fig. 9). Such an improvement in the gut microbiota diversity is considered advantageous for bolstering the efficacy of immunotherapy treatment.

We further analyzed the composition of gut microbiota at the genus level and phylum level after PGEVs treatment (Fig. 9). It is believed that an increased abundance of *Bacteroides* is related to a unsatisfactory immunotherapy response [64]. However, *Lactobacillus*, widely recognized as probiotics and frequently consumed as dietary supplements, are known to promote digestive health. The intake of *Lactobacillus fermentum* V3 as a dietary intervention may exert a regulatory effect on the gut microbiota, offering benefits in mitigating the progression of colon cancer [65]. Our data showed that the abundance of *Bacteroides* after both PGEVs treatments decreased compared to the tumor control group, and the PGEVs (oral, high) treatment resulted in a much lower abundance of *Bacteroides* than that in PGEVs (i.v., high) group. The tumor control group showed a reduction of *Lactobacillus* abundance. In contrast, the PGEVs (oral, high) treatment presented an increase in *Lactobacillus* abundance, while this increase was not as pronounced in PGEVs (i.v., high) group. The results suggest that PGEVs treatment may optimize the response to TNBC immunotherapy through decreasing the abundance of harmful bacteria *Bacteroides* and increasing the abundance of beneficial bacteria *Lactobacillus*, with oral administration being particularly efficacious. In the intestinal tract, *Firmicutes* and *Bacteroidota* represent the major groups of gram-positive and gram-negative bacterial species. Alterations in their ratio are indicative of gut dysbiosis [66]. The PGEVs (oral, high) and PGEVs (i.v., high) treatments exhibited a higher *Firmicutes/Bacteroidota* ratio in comparison with the tumor control treatment, suggesting that PGEVs treatment contribute to preserve the equilibrium of gut microbiota. Overall, PGEVs treatment improved the gut microbiota diversity, increased the beneficial bacteria abundance, and rectified dysbiosis, which is conducive to suppressing tumor growth and improving the response to TNBC immunotherapy.

Conclusions

In the present study, PGEVs were extracted from fresh PG by ultracentrifugation and sucrose gradient centrifugation method and were abundant in bioactive components. They exhibited excellent stability in simulated gastrointestinal fluid. In vitro experiments demonstrated that PGEVs could induce increased production of ROS in tumor cells, leading to tumor cell proliferation inhibition

and apoptosis, especially for a TNBC cell line 4T1. They could polarize TAMs into M1 phenotype and induce the release of pro-inflammatory cytokines. In vivo investigations revealed that PGEVs exhibited superior stability in the GIT and accumulated at tumor sites after oral administration and i.v. injection. PGEVs rebuilt the immunosuppressive TME through repolarizing TAMs to the M1 type and promoting the infiltration of CTLs, and modulated the gut microbiota, thereby achieving desirable therapeutic outcomes against TNBC. This study contributes to the advancement of effective “green” nanotherapeutics for TNBC treatment, which holds promising potential for clinical application.

Abbreviations

TNBC	Triple-negative breast cancer
PEVs	Plant-derived extracellular vesicles
PG	Platycodon grandiflorum
PGEVs	PG-derived extracellular vesicles
TAMs	Tumor-associated macrophages
TME	Tumor microenvironment
GIT	Gastrointestinal tract
CTLs	Cytotoxic T lymphocytes
SIF	Stimulated intestinal fluid
SGF	Stimulated gastric fluid
ALT	Alanine aminotransferase
AST	Aspartate aminotransferase
BUN	Urea nitrogen
CREA	Creatinine
GO	Gene Ontology
KEGG	Kyoto Encyclopedia of Genes and Genomes
PD-1	Programmed death 1

Supplementary Information

The online version contains supplementary material available at <https://doi.org/10.1186/s12951-025-03139-x>.

Supplementary Material 1

Acknowledgements

The scheme diagram was created with BioRender.com (Agreement number: LF277GDQ35).

Author contributions

Y.P. designed the experiments, supervised the studies and revised the manuscript. M.Y. designed, performed the experiments, analyzed the data, and wrote the manuscript. J.G. and Y.L. helped conduct the cell experiments and provided insightful advice for the study. J.L., S.W. and Y.S. helped extract the PGEVs and manage the mouse breeding. All the authors reviewed the final manuscript.

Funding

This work was supported by the Jilin Province Science and Technology Development Plan Project (No. YDZJ202201ZYTS443) and the Science and Technology Innovation Program of the Chinese Academy of Agricultural Sciences (No. CAAS-ASTIP-2021-ISAPS).

Data availability

No datasets were generated or analysed during the current study.

Declarations

Ethics approval and consent to participate

The animal studies were approved by the Animal Administration and Ethics Committee of the Institute of Special Animal and Plant Sciences, Chinese Academy of Agricultural Sciences (No. ISAPSAEC-2023-060PG).

Consent for publication

All the authors read and agreed to submit the manuscript.

Competing interests

The authors declare no competing interests.

Author details

¹Institute of Special Animal and Plant Sciences, Chinese Academy of Agricultural Sciences, Changchun 130112, China

²School of Chemistry and Life Science, Changchun University of Technology, Changchun 130012, China

Received: 6 September 2024 / Accepted: 19 January 2025

Published online: 07 February 2025

References

- Zhu S, Wu Y, Song B, Yi M, Yan Y, Mei Q, et al. Recent advances in targeted strategies for triple-negative breast cancer. *J Hematol Oncol*. 2023;16:100.
- Capuzzo M, Celotto V, Santorsola M, Fabozzi A, Landi L, Ferrara F, et al. Emerging treatment approaches for triple-negative breast cancer. *Med Oncol*. 2023;41:5.
- Liu Y, Hu Y, Xue J, Li J, Yi J, Bu J, et al. Advances in immunotherapy for triple-negative breast cancer. *Mol Cancer*. 2023;22:145.
- Michaels E, Chen N, Nanda R. The role of Immunotherapy in Triple-negative breast Cancer (TNBC). *Clin Breast Cancer*. 2024;24:263–70.
- Liang H, Yin G, Feng D, Chen H, Liu X, Li J. Research trends on nanomaterials in triple negative breast cancer (TNBC): a bibliometric analysis from 2010 to 2024. *Drug Deliv Transl Res*. 2024. <https://doi.org/10.1007/s13346-024-01704-9>.
- Yang M, Liu Y, Wang M, Yang C, Sun S, Zhang Q, et al. Biomineralized Gd/Dy composite nanoparticles for enhanced tumor photoablation with precise T/T-MR/CT/thermal imaging guidance. *Chem Eng J*. 2020;391:123562.
- Munir MU. Nanomedicine penetration to tumor: challenges, and advanced strategies to tackle this issue. *Cancers (Basel)*. 2022;14:2904.
- Chen Q, Zu M, Gong H, Ma Y, Sun J, Ran S, et al. Tea leaf-derived exosome-like nanotherapeutics retard breast tumor growth by pro-apoptosis and microbiota modulation. *J Nanobiotechnol*. 2023;21:6.
- Kim J, Zhu Y, Chen S, Wang D, Zhang S, Xia J, et al. Anti-glioma effect of ginseng-derived exosomes-like nanoparticles by active blood-brain-barrier penetration and tumor microenvironment modulation. *J Nanobiotechnol*. 2023;21:253.
- Xu Z, Xu Y, Zhang K, Liu Y, Liang Q, Thakur A, et al. Plant-derived extracellular vesicles (PDEVs) in nanomedicine for human disease and therapeutic modalities. *J Nanobiotechnol*. 2023;21:114.
- Ambrosone A, Barbulova A, Cappetta E, Cillo F, De Palma M, Ruocco M et al. Plant Extracellular vesicles: current Landscape and future directions. *Plants (Basel)*. 2023; 12.
- Yang M, Wang X, Pu F, Liu Y, Guo J, Chang S, et al. Engineered exosomes-based Photothermal Therapy with MRI/CT Imaging Guidance enhances Anticancer Efficacy through Deep Tumor Nucleus Penetration. *Pharmaceutics*. 2021;13:1593.
- He C, Zheng S, Luo Y, Wang B. Exosome Theranostics: Biology and Translational Medicine. *Theranostics*. 2018;8:237–55.
- Wu M, Ouyang Y, Wang Z, Zhang R, Huang PH, Chen C, et al. Isolation of exosomes from whole blood by integrating acoustics and microfluidics. *Proc Natl Acad Sci U S A*. 2017;114:10584–9.
- Zhan W, Deng M, Huang X, Xie D, Gao X, Chen J, et al. Pueraria lobata-derived exosome-like nanovesicles alleviate osteoporosis by enhancing autophagy. *J Control Release*. 2023;364:644–53.
- Yang LY, Li CQ, Zhang YL, Ma MW, Cheng W, Zhang GJ. Emerging drug delivery vectors: Engineering of Plant-Derived nanovesicles and their applications in Biomedicine. *Int J Nanomed*. 2024;19:2591–610.

17. Cao M, Yan H, Han X, Weng L, Wei Q, Sun X, et al. Ginseng-derived nanoparticles alter macrophage polarization to inhibit melanoma growth. *J Immunother Cancer*. 2019;7:326.
18. Chen Q, Li Q, Liang Y, Zu M, Chen N, Canup B, et al. Natural exosome-like nanovesicles from edible tea flowers suppress metastatic breast cancer via ROS generation and microbiota modulation. *Acta Pharm Sin B*. 2022;12:907–23.
19. Sheng Y, Liu G, Wang M, Lv Z, Du P. A selenium polysaccharide from *Platycodon grandiflorum* rescues PC12 cell death caused by H₂O₂ via inhibiting oxidative stress. *Int J Biol Macromol*. 2017;104:393–9.
20. Wang C, Schuller LG, Lee EB, Levis WR, Lee DW, Kim BS, et al. Platycodin D and D3 isolated from the root of *Platycodon grandiflorum* modulate the production of nitric oxide and secretion of TNF- α in activated RAW 264.7 cells. *Int Immunopharmacol*. 2004;4:1039–49.
21. Seo YS, Kang OH, Kong R, Zhou T, Kim SA, Ryu S, et al. Polygalacin D induces apoptosis and cell cycle arrest via the PI3K/Akt pathway in non-small cell lung cancer. *Oncol Rep*. 2018;39:1702–10.
22. Xu C, Sun G, Yuan G, Wang R, Sun X. Effects of platycodin D on proliferation, apoptosis and PI3K/Akt signal pathway of human glioma U251 cells. *Molecules*. 2014;19:21411–23.
23. Li T, Chen X, Chen X, Ma DL, Leung CH, Lu JJ. Platycodin D potentiates proliferation inhibition and apoptosis induction upon AKT inhibition via feedback blockade in non-small cell lung cancer cells. *Sci Rep*. 2016;6:37997.
24. Chen D, Chen T, Guo Y, Wang C, Dong L, Lu C. Platycodin D (PD) regulates LncRNA-XIST/miR-335 axis to slow down bladder cancer progression in vitro and in vivo. *Exp Cell Res*. 2020;396:112281.
25. Yoon YD, Han SB, Kang JS, Lee CW, Park SK, Lee HS, et al. Toll-like receptor 4-dependent activation of macrophages by polysaccharide isolated from the radix of *Platycodon grandiflorum*. *Int Immunopharmacol*. 2003;3:1873–82.
26. Chun YB. Regulatory effects of Crotonin, Platycodin D, Peimine and their compatibility on immune cells in gastric cancer. *Nanjing University of Chinese Medicine*; 2021.
27. Yang RJ. Study on the main active ingredients of *Platycodon grandiflorum* trigger anti-tumor mechanism through immune regulation. *Northwest University*; 2021.
28. Kwon M, Ji HK, Goo SH, Nam SJ, Kang YJ, Lee E, et al. Involvement of intestinal efflux and metabolic instability in the pharmacokinetics of platycodin D in rats. *Drug Metab Pharmacokinet*. 2017;32:248–54.
29. Rasoanaivo P, Wright CW, Willcox ML, Gilbert B. Whole plant extracts versus single compounds for the treatment of malaria: synergy and positive interactions. *Malar J*. 2011;10(Suppl 1):S4.
30. Yang M, Guo J, Fang L, Chen Z, Liu Y, Sun Z, et al. Quality and efficiency assessment of five extracellular vesicle isolation methods using the resistive pulse sensing strategy. *Anal Methods-Uk*. 2024;16:5536–44.
31. Zeng L, Wang H, Shi W, Chen L, Chen T, Chen G, et al. Aloe derived nanovesicle as a functional carrier for indocyanine green encapsulation and phototherapy. *J Nanobiotechnol*. 2021;19:439.
32. Simbari F, McCaskill J, Coakley G, Millar M, Maizels RM, Fabrias G, et al. Plasmalogen enrichment in exosomes secreted by a nematode parasite versus those derived from its mouse host: implications for exosome stability and biology. *J Extracell Vesicles*. 2016;5:30741.
33. Popova AV, Hinch DK. Intermolecular interactions in dry and rehydrated pure and mixed bilayers of phosphatidylcholine and digalactosyldiacylglycerol: a Fourier transform infrared spectroscopy study. *Biophys J*. 2003;85:1682–90.
34. Zhang H, Xiao Y, Cui S, Zhou Y, Zeng K, Yan M, et al. Novel Galactosylated Poly(ethylene glycol)-Cholesterol for liposomes as a drug carrier for hepatocyte-targeting. *J Nanosci Nanotechnol*. 2015;15:4058–69.
35. Rome S. Biological properties of plant-derived extracellular vesicles. *Food Funct*. 2019;10:529–38.
36. Pinedo M, de la Canal L, de Marcos LC. A call for Rigor and standardization in plant extracellular vesicle research. *J Extracell Vesicles*. 2021;10:e12048.
37. He B, Cai Q, Qiao L, Huang CY, Wang S, Miao W, et al. RNA-binding proteins contribute to small RNA loading in plant extracellular vesicles. *Nat Plants*. 2021;7:342–52.
38. Duan B, Zou S, Sun Y, Xu X. Fabrication of tumor-targeting composites based on the triple helical beta-glucan through conjugation of aptamer. *Carbohydr Polym*. 2021;254:117476.
39. Stepanic V, Gasparovic AC, Troselj KG, Amic D, Zarkovic N. Selected attributes of polyphenols in targeting oxidative stress in cancer. *Curr Top Med Chem*. 2015;15:496–509.
40. Yang M, Pu L, Yang S, Chen Z, Guo J, Liu Y, et al. Engineered antler stem cells derived exosomes potentiate anti-tumor efficacy of immune checkpoint inhibitor by reprogramming immunosuppressive tumor microenvironment. *Chem Eng J*. 2024;479:147421.
41. Barnes NG. Targeting TAMs. *Nat Rev Chem*. 2022;6:678.
42. Geels SN, Moshensky A, Sousa RS, Murat C, Bustos MA, Walker BL, et al. Interruption of the intratumor CD8(+) T cell:Treg crosstalk improves the efficacy of PD-1 immunotherapy. *Cancer Cell*. 2024;42:1051–66.
43. Zhou D, Li Y. Gut microbiota and tumor-associated macrophages: potential in tumor diagnosis and treatment. *Gut Microbes*. 2023;15:2276314.
44. Wu M, Bai J, Ma C, Wei J, Du X. The Role of Gut Microbiota in Tumor Immunotherapy. *J Immunol Res*. 2021;2021: 5061570.
45. Wang Q, Lv L, Jiang H, Wang K, Yan R, Li Y, et al. *Lactobacillus helveticus* R0052 alleviates liver injury by modulating gut microbiome and metabolome in D-galactosamine-treated rats. *Appl Microbiol Biotechnol*. 2019;103:9673–86.
46. Alfieri M, Leone A, Ambrosone A. Plant-derived nano and microvesicles for human health and therapeutic potential in nanomedicine. *Pharmaceutics*. 2021;13:498.
47. Zheng M, Chavda VP, Vaghela DA, Bezbaruah R, Gogoi NR, Patel K, et al. Plant-derived exosomes in therapeutic nanomedicine, paving the path toward precision medicine. *Phytomedicine*. 2024;135:156087.
48. Yang M, Luo Q, Chen X, Chen F. Bitter melon derived extracellular vesicles enhance the therapeutic effects and reduce the drug resistance of 5-fluorouracil on oral squamous cell carcinoma. *J Nanobiotechnol*. 2021;19:259.
49. Cui WW, Ye C, Wang KX, Yang X, Zhu PY, Hu K, et al. *Momordica*. Charantia-derived extracellular vesicles-like Nanovesicles Protect Cardiomyocytes against Radiation Injury via attenuating DNA damage and Mitochondria Dysfunction. *Front Cardiovasc Med*. 2022;9:864188.
50. Ma X, Shao S, Xiao F, Zhang H, Zhang R, Wang M, et al. *Platycodon grandiflorum* extract: chemical composition and whitening, antioxidant, and anti-inflammatory effects. *Rsc Adv*. 2021;11:10814–26.
51. Li T, Xu XH, Tang ZH, Wang YF, Leung CH, Ma DL, et al. Platycodin D induces apoptosis and triggers ERK- and JNK-mediated autophagy in human hepatocellular carcinoma BEL-7402 cells. *Acta Pharmacol Sin*. 2015;36:1503–13.
52. An X, Yu W, Liu J, Tang D, Yang L, Chen X. Oxidative cell death in cancer: mechanisms and therapeutic opportunities. *Cell Death Dis*. 2024;15:556.
53. Redza-Dutordoir M, Averill-Bates DA. Activation of apoptosis signalling pathways by reactive oxygen species. *Biochim Biophys Acta*. 2016;1863:2977–92.
54. Yang M, Liu X, Luo Q, Xu L, Chen F. An efficient method to isolate lemon derived extracellular vesicles for gastric cancer therapy. *J Nanobiotechnol*. 2020;18:100.
55. Dallavalasa S, Beeraka NM, Basavaraju CG, Tulimilli SV, Sadhu SP, Rajesh K, et al. The role of Tumor Associated macrophages (TAMs) in Cancer Progression, Chemoresistance, Angiogenesis and Metastasis - Current Status. *Curr Med Chem*. 2021;28:8203–36.
56. Kzhyshkowska J, Shen J, Larionova I. Targeting of TAMs: can we be more clever than cancer cells? *Cell Mol Immunol*. 2024;21:1376–409.
57. Khabipov A, Kading A, Liedtke KR, Freund E, Partecke LI, Bekeschus S. RAW 264.7 macrophage polarization by pancreatic Cancer cells - a model for studying Tumour-promoting macrophages. *Anticancer Res*. 2019;39:2871–82.
58. He S, Wang S, Liu S, Li Z, Liu X, Wu J. Baicalein Potentiated M1 Macrophage polarization in Cancer through Targeting PI3Kgamma/ NF-kappaB signaling. *Front Pharmacol*. 2021;12:743837.
59. Wei W, Li ZP, Bian ZX, Han QB. Astragalus polysaccharide RAP induces macrophage phenotype polarization to M1 via the notch signaling pathway. *Molecules*. 2019;24:2016.
60. Lu Y, Yuan X, Wang M, He Z, Li H, Wang J, et al. Gut microbiota influence immunotherapy responses: mechanisms and therapeutic strategies. *J Hematol Oncol*. 2022;15:47.
61. Zhao LY, Mei JX, Yu G, Lei L, Zhang WH, Liu K, et al. Role of the gut microbiota in anticancer therapy: from molecular mechanisms to clinical applications. *Signal Transduct Target Ther*. 2023;8:201.
62. Zitvogel L, Ma Y, Raouf D, Kroemer G, Gajewski TF. The microbiome in cancer immunotherapy: diagnostic tools and therapeutic strategies. *Science*. 2018;359:1366–70.
63. Jin Y, Dong H, Xia L, Yang Y, Zhu Y, Shen Y, et al. The diversity of gut microbiome is Associated with favorable responses to Anti-programmed Death 1 immunotherapy in Chinese patients with NSCLC. *J Thorac Oncol*. 2019;14:1378–89.
64. Peters BA, Wilson M, Moran U, Pavlick A, Izsak A, Wechter T, et al. Relating the gut metagenome and metatranscriptome to immunotherapy responses in melanoma patients. *Genome Med*. 2019;11:61.

65. Chou YC, Ho PY, Chen WJ, Wu SH, Pan MH. *Lactobacillus fermentum* V3 ameliorates colitis-associated tumorigenesis by modulating the gut microbiome. *Am J Cancer Res.* 2020;10:1170–81.
66. Di Vincenzo F, Del GA, Petito V, Lopetuso LR, Scaldaferrri F. Gut microbiota, intestinal permeability, and systemic inflammation: a narrative review. *Intern Emerg Med.* 2024;19:275–93.

Publisher's note

Springer Nature remains neutral with regard to jurisdictional claims in published maps and institutional affiliations.